Subcytoplasmic location of translation controls protein output

Ellen L. Horste[1,2], Gang Zhen[2], Mervin M. Fansler[2,3], Xiuzhen Chen[2], Flora C. Y. Lee[4,5], Jernej Ule[4,5], and Christine Mayr[1,2,3†]

[1]Gerstner Sloan Kettering Graduate School of Biomedical Sciences, New York, NY 10065, USA
[2]Cancer Biology and Genetics Program, Sloan Kettering Institute, New York, NY 10065, USA
[3]Tri-Institutional Training Program in Computational Biology and Medicine, Weill-Cornell Graduate College, New York, NY 10021, USA
[4]UK Dementia Research Institute, King's College London, London, SE5 9NU, UK
[5]The Francis Crick Institute, 1 Midland Road, London NW1 1AT, UK

[†]Correspondence: mayrc@mskcc.org

Summary

The cytoplasm is highly compartmentalized, but the extent of subcytoplasmic mRNA localization in non-polarized cells is largely unknown. We used fluorescent particle sorting to determine mRNA enrichment in three unenclosed cytoplasmic compartments: the canonical rough endoplasmic reticulum (CRER), the TIS granule-associated rough endoplasmic reticulum (TGER), and the cytosol. Focusing our analysis on non-membrane protein-encoding mRNAs, we observed that 53% have a unique subcytoplasmic localization pattern which is determined by a combinatorial code of 3′UTR-bound RNA-binding proteins. Compartment-enriched mRNAs differed in production and degradation rates and the expression levels and functional classes of their encoded proteins. The TGER domain enriches mRNAs that encode transcription factors, the CRER highly expressed proteins, and the cytosol unstable mRNAs. The rough ER environment is stimulatory as redirecting cytosolic mRNAs to the ER increases their protein expression by two-fold, independently of the bound RNA-binding proteins. We show that local translation environments functionally compartmentalize the cytoplasm.

Keywords

Cytoplasmic organization, spatial regulation, mRNA localization, unenclosed cytoplasmic compartments, subdomains of the endoplasmic reticulum, ER subdomains, translation environment, regulation of protein expression, condensates, rough endoplasmic reticulum membrane, 3′UTRs, RNA-binding proteins, CLIP analysis, TIS11B, TIAL1, LARP4B

Introduction

In polarized cells such as neurons, intestinal epithelial cells, or cells of the early fly embryo, the majority of mRNAs have a distinct spatial localization pattern (Huttelmaier et al., 2005; Lecuyer et al., 2007; Moor et al., 2017; Tushev et al., 2018; Glock et al., 2021), which enables the local control of protein production and activity (Moretti et al., 2015; Buxbaum et al., 2015; Biever et al., 2019).

In non-polarized cells, local protein synthesis has primarily been studied for membrane and secretory proteins, which are predominantly translated on the endoplasmic reticulum (ER) (Reid and Nicchitta, 2012; Jan et al., 2014; Fazal et al., 2019). However, the cytoplasm is highly compartmentalized by additional membrane-bound and membraneless organelles (Banani et al., 2017; Shin and Brangwynne, 2017; Ma and Mayr, 2018). Compartmentalization allows

reactions to occur in parallel and may enable the generation of unique biochemical translation environments (Ma and Mayr, 2018; Peeples and Rosen, 2021). Subcellular localization within the cytoplasm was observed for specific mRNAs enriched on the mitochondrial surface (Fazal et al., 2019; Qin et al., 2021). However, but it is currently largely unknown to what extent mRNAs that encode non-membrane proteins differentially localize to the ER or the cytosol or if the amount of protein synthesis differs depending on the subcytoplasmic location of an mRNA.

We recently discovered a cytoplasmic condensate, called TIS granule network, that is generated through assembly of the RNA-binding protein TIS11B together with its bound mRNAs (Ma and Mayr, 2018). According to single cell RNA-seq data, *TIS11B* mRNA is expressed in more than 100 human cell types and was detected in all cell types analyzed, suggesting that TIS granules are widespread (Han et al., 2020). TIS granules are present under steady-state cultivation conditions and form a network-like structure that is associated with the surface of the rough ER (Ma and Mayr, 2018; Ma et al., 2021). With respect to their functions, it was shown that translation of specific mRNAs in TIS granules allows assembly of protein complexes that cannot be established when the mRNAs are translated on the ER but outside of TIS granules (Ma and Mayr, 2018). These results suggested that the rough ER contains two functional domains, the canonical rough ER (CRER) and the TIS granule ER (TGER).

To investigate the broader biological significance of TIS granules, we set out to determine the mRNAs enriched in the two rough ER domains and in the surrounding cytosol. Several methods were developed to investigate subcellular transcriptomics. They include RNA sequencing (RNA-seq) after biochemical fractionation, APEX-seq, MERFISH, and fluorescent particle sorting (Mili et al., 2008; Hubstenberger et al., 2017; Khong et al., 2017; Moor et al., 2017; Xia et al., 2019; Fazal et al., 2019). Application of these methods identified mRNAs that localize to cellular protrusions of migrating fibroblasts and distinguished between mRNAs that localize to the apical or basal sides of gut epithelial cells (Mili et al., 2008; Moor et al., 2017). These methods also determined the transcriptomes of cytoplasmic condensates such as P bodies or stress granules (Hubstenberger et al., 2017; Khong et al., 2017) and identified mRNAs associated with membrane-bound organelles such as the ER or mitochondria (Fazal et al., 2019; Qin et al., 2021). To identify mRNAs enriched in TIS granules, we used fluorescent particle sorting (Hubstenberger et al., 2017). This decision was based on the observation that TIS11B protein (also called ZFP36L1) is present in cells in two assembly states. It exists in an unassembled state in the cytosol and assembles together with its bound mRNAs into TIS granules (Fig. 1A) (Ma and Mayr, 2018; Ma et al., 2021).

We applied fluorescent particle sorting to isolate TGER and CRER-associated mRNAs and compared them with digitonin-extracted cytosolic mRNAs. In addition to ~1,700 mRNAs that encode membrane proteins, we detected more than 2,100 mRNAs that encode non-membrane proteins enriched in the two rough ER domains, indicating that the ER membrane is a general translation compartment and is not restricted to membrane and secretory proteins. We focused our analysis on mRNAs that encode non-membrane proteins. For more than half of them, we observed enrichment in one of the three subcytoplasmic compartments. The localization pattern was largely controlled by a combinatorial code of the 3′UTR-bound RNA-binding proteins TIS11B, TIA1/L1, and LARP4B. Compartment-enriched mRNAs differed substantially in their production and degradation rates as well as in the functional classes and expression levels of their encoded proteins. In addition to RNA-binding proteins, we found that the location of translation has an independent effect on protein expression. We observed that redirecting cytosolic mRNAs to the rough ER membrane increased their steady-state protein expression levels by two-fold, indicating a strong stimulatory effect of the ER environment on protein output.

Results

Approach to determine subcytoplasmic mRNA localization

We set out to study differential mRNA localization across three major unenclosed cytoplasmic compartments in non-polarized human HEK293T cells under steady-state cultivation conditions. We determined the mRNAs enriched at the cytosolic surface of the ER – the largest cytoplasmic organelle, TIS granules, an ER-associated condensate network, and the cytosol (Fig. 1B). For simplicity, we consider here the sum of the three compartments as the universe of cytoplasmic mRNAs.

To identify TIS granule-localized mRNAs, we used fluorescent particle sorting followed by RNA-seq. After transfecting cells with fluorescently tagged TIS11B to label TIS granules, we used mechanical lysis and differential centrifugation to isolate the cytoplasmic membrane fraction which was followed by flow cytometry-based sorting of TIS11B-positive particles (Fig. S1A, S1B). DAPI staining allowed us to identify and discard nuclei that were still associated with the ER and TIS granules and to isolate TIS11B-positive particles free of nuclei. To investigate if the obtained particles were pure TIS granules or if they contained ER membrane, we double-labeled TIS granules and the rough ER membrane, followed by particle sorting and confocal microscopy. This revealed that the TIS11B-positive particles cannot be separated from the rough ER membrane and therefore, we call them TIS granule ER (TGER) particles (Fig. 1C).

To isolate the canonical rough ER (CRER), we labeled the rough ER membrane with fluorescently tagged SEC61B and isolated CRER particles with the same strategy. We obtained particles similar in size to TGER particles (Fig. 1C, Fig. S1C). To isolate cytosolic mRNAs, we used digitonin extraction (Liu and Fagotto, 2011). The extracted cytosol was not contaminated by nuclei or the ER, but it contained cytosolic proteins, including unassembled TIS11B protein and GAPDH which was used as positive control (Fig. S1D).

We performed RNA-seq to determine the mRNAs in the three fractions and focused our analysis on protein-coding mRNAs. Previous analyses showed that most mRNAs that encode membrane or secretory proteins are translated on the ER, whereas mRNAs that encode non-membrane proteins are translated in the cytosol (Jan et al., 2014; Fazal et al., 2019). Consistent with this, we observed distinct partitioning patterns between the two groups across the three compartments (Fig. S1E).

mRNAs that encode membrane and secretory proteins are strongly enriched on the CRER membrane

Based on the different partitioning patterns, we analyzed the mRNAs that encode membrane or secretory proteins separately from the mRNAs that encode non-membrane proteins. Proteins that contain either a signal sequence or transmembrane domain are defined as secretory or membrane proteins and are encoded by 23% of mRNAs expressed in HEK293T cells, whereas the remaining 77% encode non-membrane proteins. We determined the compartment-specific partition coefficients in each group: For each gene, we calculated the fraction of mRNA transcripts that localize to TGER, the CRER, or the cytosol and observed the expected baseline distributions across the three compartments (Fig. S1E).

For mRNAs that encode membrane/secretory proteins, we observed 69% (N = 1,476) to be specifically enriched at the CRER (Fig. S1F). When comparing the CRER membrane-enriched mRNAs with analyses from alternative isolation methods, we detected approximately 80% overlap among the ER membrane-enriched mRNAs, supporting the validity of our purification strategy (Fig. S1G) (Reid and Nicchitta, 2012; Fazal et al., 2019).

Horste et al., Figure 1

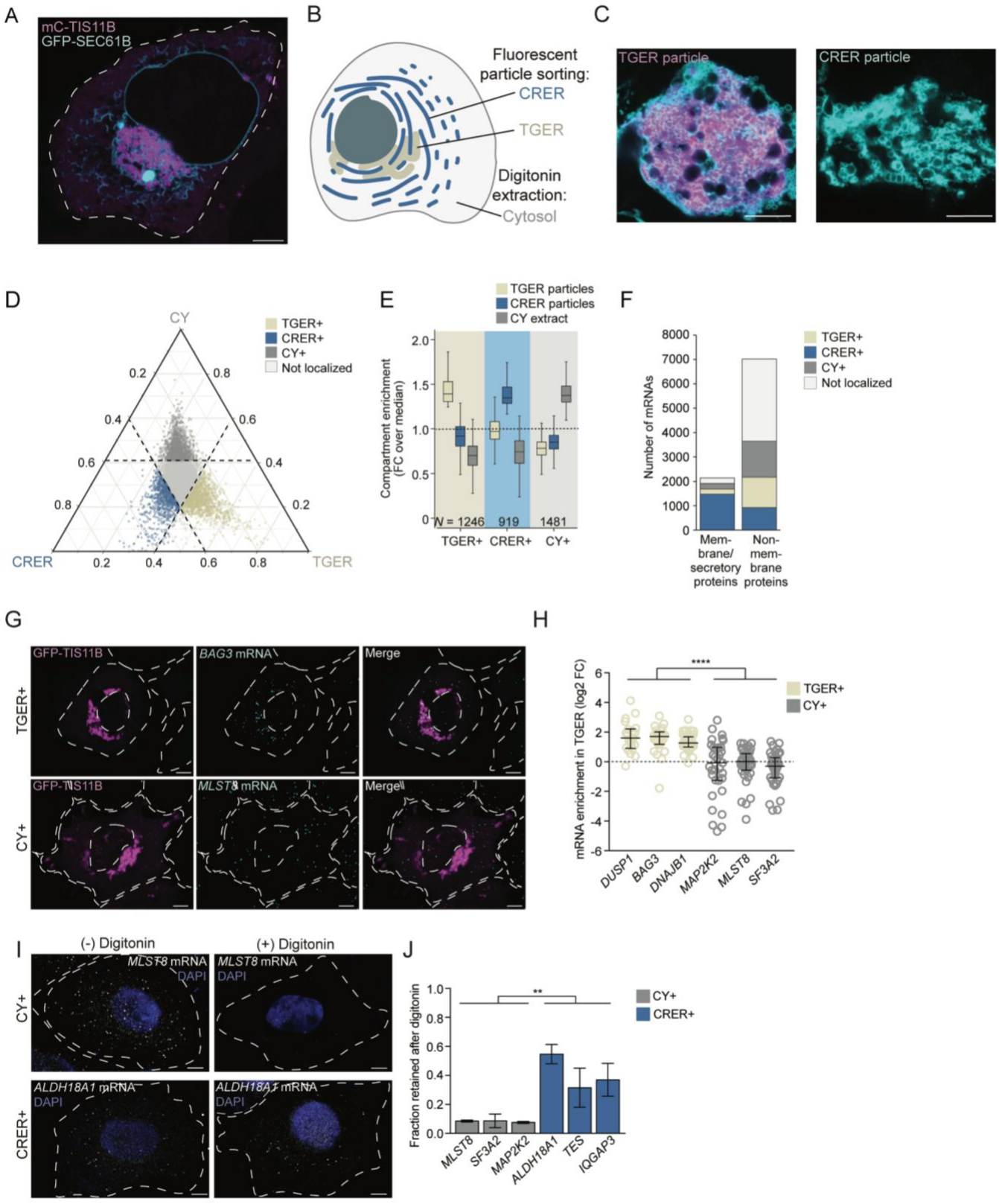

Figure 1. Strategy to determine subcytoplasmic mRNA localization.
(A) Confocal live cell imaging of HeLa cells after transfection of mCherry (mC)-TIS11B (magenta) to visualize TIS granules and of GFP-SEC61B to visualize the rough ER (teal). Scale bar, 5 µm.
(B) Schematic showing purification strategy to identify mRNAs within three cytoplasmic compartments, including TGER (beige), CRER (blue), and the cytosol (grey).
(C) As in (A), but after sorting of fluorescent particles. Shown is a TGER particle (left) and a CRER particle (right). Scale bar, 5 µm.
(D) Ternary plot showing compartment-specific enrichment of mRNAs that encode non-membrane proteins. Each dot represents an mRNA color-coded as in (B). TGER-enriched (TGER+), *N* = 1246, CRER+, *N* = 919, cytosol-enriched (CY+), *N* = 1481 mRNAs. mRNAs without a unique subcytoplasmic location are in the center (not localized, light grey, *N* = 3369).
(E) As in (D) but shown is the compartment-specific enrichment of mRNAs that are overrepresented in single cytoplasmic compartments. Compartment enrichment is the fold change (FC) of each mRNA-specific partition coefficient normalized by the median partition coefficient of each fractionation sample.
(F) The number of compartment-enriched mRNAs is shown separately for mRNAs that encode membrane or secretory proteins versus non-membrane proteins.
(G) Single-molecule (sm) RNA-FISH of the indicated endogenous mRNAs (teal) in HeLa cells. TIS granules were visualized by using GFP-TIS11B (magenta). Cell and nuclear boundaries are indicated by the dotted lines. Representative images are shown. Scale bar, 5 µm.
(H) Quantification of (G). Colocalization of smRNA-FISH foci and TIS granules was determined. Shown is the log2 fold-change (FC) of the observed over expected TGER localization based on the relative area of TIS granules and the cytosol in each cell. Each cell is represented by one dot and the summarized data from three independent experiments is shown. Number of cells analyzed, *DUSP1*, *N* = 21; *BAG3*, *N* = 25; *DNAJB1, N* = 32; *MAP2K2, N* = 45; *MLST8, N* = 38; *SF3A2, N* = 37. Representative images are shown in Fig. S1I and S1J. Differential localization between TGER+ and CY+ mRNAs: Mann-Whitney test, ****, *P* = 3 E-20. *SF3A2* mRNA is significantly depleted from TIS granules, Mann-Whitney test, *P* = 0.004.
(I) Shown are smRNA-FISH foci of endogenous mRNAs in HeLa cells before (-) and after (+) digitonin treatment. Cell and nuclear boundaries are indicated by the dotted lines. Representative images are shown. Scale bar, 5 µm.
(J) Quantification of (I). Shown is the fraction of digitonin-resistant smRNA-FISH foci of endogenous mRNAs as mean ± std of three independent experiments. Number of cells analyzed, *MLST8, N* = 70; *SF3A2, N* = 67; *MAP2K2, N* = 48; *ALDH18A1, N* = 63; *TES, N* = 81; *IQGAP3, N* = 50. Representative images are shown in Fig. S1K and S1L. T-test for independent samples, **, *P* = 0.008.

mRNAs that encode non-membrane proteins are widely enriched on the rough ER

For mRNAs that encode non-membrane proteins, we observed a more evenly distributed baseline partitioning across the three compartments with roughly a third of transcripts localizing to TGER, CRER or to the cytosol (Fig. S1E). We considered an mRNA to be compartment-enriched when its enrichment coefficient was greater than 1.25 (Fig. S1H). This means that an mRNA is compartment-enriched if the fraction of transcripts that localize to one compartment is 1.25-fold higher than the median fraction observed in the compartment. With this strategy, we identified 1246 mRNAs enriched in the TGER domain, 919 non-overlapping mRNAs enriched on the CRER surface, and 1481 mRNAs enriched in the cytosol. The remaining 3369 mRNAs had either no subcellular localization preference or localized to two out of the three compartments (Fig. 1D, Table S1). The enrichment is relative, as for mRNAs considered to be enriched in CRER, the median fraction of compartment-localized transcripts is 41% whereas for the TGER and the cytosol, it is 47% (Fig. 1E). Overall, we found that 53% of mRNAs that encode non-membrane proteins to be enriched in a single subcytoplasmic compartment in steady-state conditions of non-polarized cells.

Taken together, for the two rough ER domains, we found enrichment of mRNAs that encode membrane or secretory proteins, but we detected even more mRNAs that encode non-

membrane proteins enriched (Fig. 1F). Dozens of these mRNAs have been found previously by several other groups (Lerner et al., 2003; Diehn et al., 2006; Chen et al., 2011; Reid and Nicchitta, 2012; Cui et al., 2012; Voigt et al., 2017) but the extent of localization of mRNAs that encode non-membrane proteins to the rough ER was previously unknown. This suggests that the rough ER membrane is a general translation compartment not restricted to membrane or secretory proteins. All remaining analyses were performed on mRNAs that encode non-membrane proteins.

Validation of subcytoplasmic mRNA localization patterns by single-molecule RNA-FISH

To validate mRNA localization across the three compartments, we performed single-molecule (sm) RNA-FISH on endogenous mRNAs predicted to localize to TGER or to the cytosol (Boraas et al., 2021). The TGER domain was visualized using fluorescently tagged TIS11B. Based on the area occupied by TGER or the cytosol in each cell, we calculated the expected distribution of mRNA foci across the two compartments. To identify compartment-enriched mRNAs, we determined the fold-change between the observed and expected number of mRNA foci in each compartment. Our smRNA-FISH experiment confirmed TGER enrichment of all candidates predicted to be overrepresented in the TGER domain. mRNAs predicted to be enriched in the cytosol were not enriched in the TGER domain and were even excluded from the TGER domain in some samples (Fig. 1G, 1H, S1I, S1J, Table S2).

The fine reticulated structure of the ER membrane makes it challenging to perform a similar colocalization analysis for the CRER. ER-localized mRNAs are tethered to the ER and are relatively resistant to digitonin extraction compared to cytosolic mRNAs (Lerner et al., 2003; Cui et al., 2012). To validate the enrichment of mRNAs on the CRER, we performed smRNA-FISH before and after digitonin extraction and calculated the fraction of retained mRNAs. We observed significantly higher retention rates for mRNAs predicted to be CRER-localized compared to mRNAs predicted to be cytosolic (Fig. 1I, 1J, S1K, S1L, Table S2). Based on our high validation rates for mRNAs that localize to the three investigated cytoplasmic compartments, we conclude that about half (53%) of mRNAs that encode non-membrane proteins preferentially localize to a single subcytoplasmic location.

mRNA and protein levels strongly correlate with the location of translation

Next, we characterized the features of compartment-enriched mRNAs and found substantial differences in their steady-state mRNA and protein levels (Fig. 2A, 2B). We observed that TGER-enriched mRNAs have the lowest steady-state expression levels and encode proteins with the lowest expression levels (Fig. 2A, 2B). To examine if the low mRNA levels are caused by mRNA degradation, we estimated mRNA half-lives by analyzing Precision Run-On sequencing (Pro-seq) and RNA-seq data (Fig. 2C, 2D, Fig. S2A) (Patel et al., 2020; Blumberg et al., 2021). Pro-seq values can be treated as transcription rates and RNA-seq data can be viewed as a measure of RNA concentration to estimate RNA decay rates required for a steady-state equilibrium (Blumberg et al., 2021). For TGER-enriched mRNAs, we observed that the low steady-state mRNA levels are not primarily caused by a low mRNA stability. Instead, these mRNAs had the lowest transcription rates which suggests that these mRNAs are either produced at a low rate or have high cotranscriptional degradation rates (Fig. 2C, 2D) (Smalec et al., 2022).

CRER-enriched mRNAs had higher production and stability values and encode proteins with the highest expression levels (Fig. 2A-D). In contrast, mRNAs enriched in the cytosol showed the highest degree of mRNA regulation with high production and high degradation rates which is consistent with the highest steady-state mRNA expression levels and lower expression of their encoded proteins (Fig. 2A-D). The compartment-enriched mRNAs also showed differences in their gene architectures. Compared with cytosolic mRNAs, mRNAs enriched on the rough ER

have longer 3′UTRs that are AU-rich and contain higher numbers of AU-rich elements (Fig. S2B-D). Furthermore, CRER-enriched mRNAs encode the largest proteins which are more than twice as large as proteins encoded by cytosolic mRNAs (Fig. S2E).

Consistent with the observed differences in steady-state protein expression levels, compartment-enriched mRNAs encode substantially different functional gene classes (Huang da et al., 2009). TGER-localized mRNAs are strongly enriched in zinc fingers and transcription factors (Fig. 2E). CRER-localized mRNAs are enriched in helicases, cytoskeleton-binding proteins and chromatin regulators which represent large proteins that require high expression levels (Fig. 2F). Cytosolic mRNAs often encode smaller proteins involved in the regulation of translation and splicing (Fig. 2G).

Horste et al., Figure 2

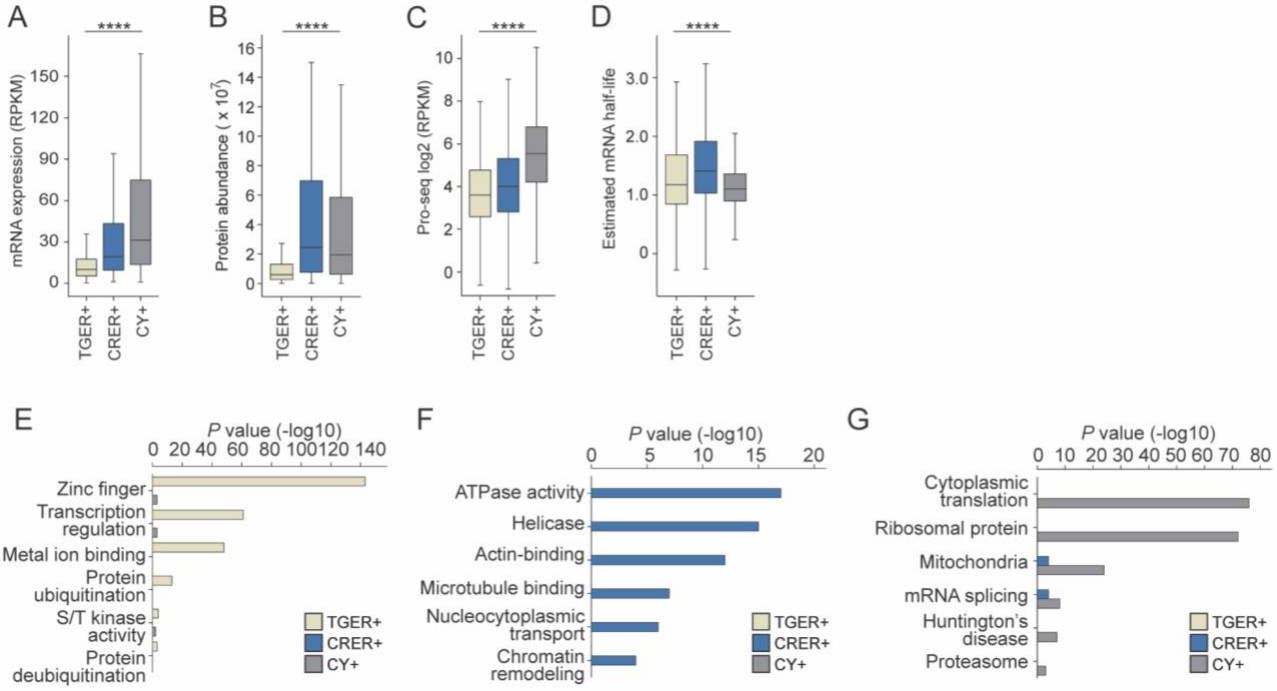

Figure 2. Characteristics of compartment-enriched mRNAs.
(A) Steady-state mRNA abundance levels obtained from whole cell lysates measured by RNA-seq for compartment-enriched mRNAs. TGER+, *N* = 1246; CRER+, *N* = 919, CY+, *N* = 1481. Kruskal-Wallis test: ****, *P* = 3 E-147. TGER vs CRER, Mann-Whitney test: ****, *P* = 3 E-47. RPKM, reads per kilobase of transcript per million reads mapped.
(B) As in (A), but steady-state protein levels obtained from whole cell lysates, determined by mass spectrometry are shown. TGER+, *N* = 469, CRER+, *N* = 638, and CY+, *N* = 833. Kruskal-Wallis test: ****, *P* = 8E-52. TGER vs CRER, Mann-Whitney test: *, *P* = 0.019; CRER vs CY, Mann-Whitney test: *, *P* = 0.019.
(C) As in (A), but Pro-seq levels are shown, which indicate transcription rates. TGER+, *N* = 1222; CRER+, *N* = 896, CY+, *N* = 1425. Kruskal-Wallis test: ****, *P* = 2E-124. TGER vs CRER, Mann-Whitney test: ****, *P* = 1E-5.
(D) As in (C), but estimated mRNA half-lives are shown. Kruskal-Wallis test: ****, *P* = 5E-28. TGER vs CY, Mann-Whitney test: ****, *P* = 7E-4.
(E) Gene ontology analysis for TGER-enriched mRNAs. Shown are the top six functional gene classes and their Benjamini-Hochberg adjusted *P* values for categories that are significantly and uniquely enriched in TGER+ mRNAs. The Benjamini-Hochberg adjusted *P* values for the same categories for CRER+ and CY+ mRNAs are shown for comparison reasons.
(F) As in (E), but for CRER-enriched mRNAs.
(G) As in (E), but for mRNAs enriched in the cytosol.

The TGER domain supports active translation

Transcription factors are known to be expressed at lower abundance levels than non-transcription factors (Vaquerizas et al., 2009). Our analysis suggests that proteins, that need to be expressed in low abundance, such as transcription factors, are translated in the TGER domain (Fig. 2A, 2B, 2E). To obtain direct evidence for translation in the TGER domain, we applied the SunTag system to simultaneously visualize mRNAs and their nascent proteins in TGER and in the cytosol (Fig. S2F, S2G) (Yan et al., 2016). We used two SunTag reporters and confirmed that the TGER domain represents a translation environment for mRNAs (Ma and Mayr, 2018). For both reporters, we observed that the number of mRNA foci in TGER was five-fold lower compared to the cytosol. However, mRNA translation rates were similar in TGER and the cytosol (Fig. S2H, S2I). Taken together, our data show that the TGER translation environment is not repressive and that the low expression levels of TGER-translated proteins are predominantly a result of their low nuclear gene expression (Fig. 2A, 2C).

A combinatorial code of 3′UTR-bound RNA-binding proteins determines subcytoplasmic mRNA localization

Our next goal was to identify the RNA-binding proteins responsible for mRNA enrichment in the three compartments (Fig. 1D, 1E). As TIS11B is the scaffold protein of TIS granules, we performed iCLIP of TIS11B in HEK293T cells (Fig. S3A, S3B). We confirmed that the top binding motif of TIS11B in 3′UTRs of mRNAs is the canonical AU-rich element (UAUUUA) (Fig. S3C). To perform a comprehensive analysis on localization regulators, we analyzed additional CLIP datasets (Küspert et al., 2015; Zhao et al., 2021). Altogether, we correlated the 3′UTR binding pattern of 170 RNA-binding proteins with mRNA enrichment in the three subcytoplasmic compartments. Among them, we found that the 3′UTR CLIP peak distributions of 25 RNA-binding proteins were biased towards one of the three compartments (Table S3). We applied logistic regression and identified seven RNA-binding proteins whose binding contributed significantly to mRNA localization to the three compartments (Fig. 3A, S3D-F).

Binding of TIS11B showed the strongest positive association for mRNA localization to the TGER domain (Fig. 3A). Moreover, most mRNAs bound by HuR, PUM2 or HNRNPC were also bound by TIS11B. Although binding of these other AU-rich RNA-binding proteins was positively associated with TGER localization, the number of mRNAs exclusively bound by them is small (N = 148, Fig. S3D). We further observed that binding of METAP2 is associated with cytosolic mRNA localization, but only few mRNAs (N = 90) were bound by METAP2 alone (Fig. S3E). Therefore, for further analysis, we focused on TIS11B, TIA1/L1, and LARP4B as their 3′UTR binding pattern was most informative for mRNA localization to the three compartments (Fig. 3A). As a previous CLIP analysis showed that peaks for TIA1 and TIAL1 cannot be distinguished (Wang et al., 2010), we used the sum of peaks from TIA1 and TIAL1 to obtain the values for TIA1/L1.

3′UTR-bound TIS11B versus LARP4B is the major discriminator of mRNA localization between the rough ER and the cytosol

We separated all non-membrane protein-encoding mRNAs into eight groups based on their binding pattern of TIS11B, TIA1/L1, and LARP4B (Fig. S3F). We distinguished mRNAs exclusively bound by one of the three or cobound by pairs of RNA-binding proteins. This analysis recapitulated the results of the logistic regression and revealed that the binding pattern of TIS11B and LARP4B is associated with opposite effects on cytoplasmic mRNA localization. Binding of LARP4B correlates with cytosolic mRNA localization, whereas binding of TIS11B is associated with rough ER localization with a preference for TGER (Fig. 3B, 3C). Cobinding of

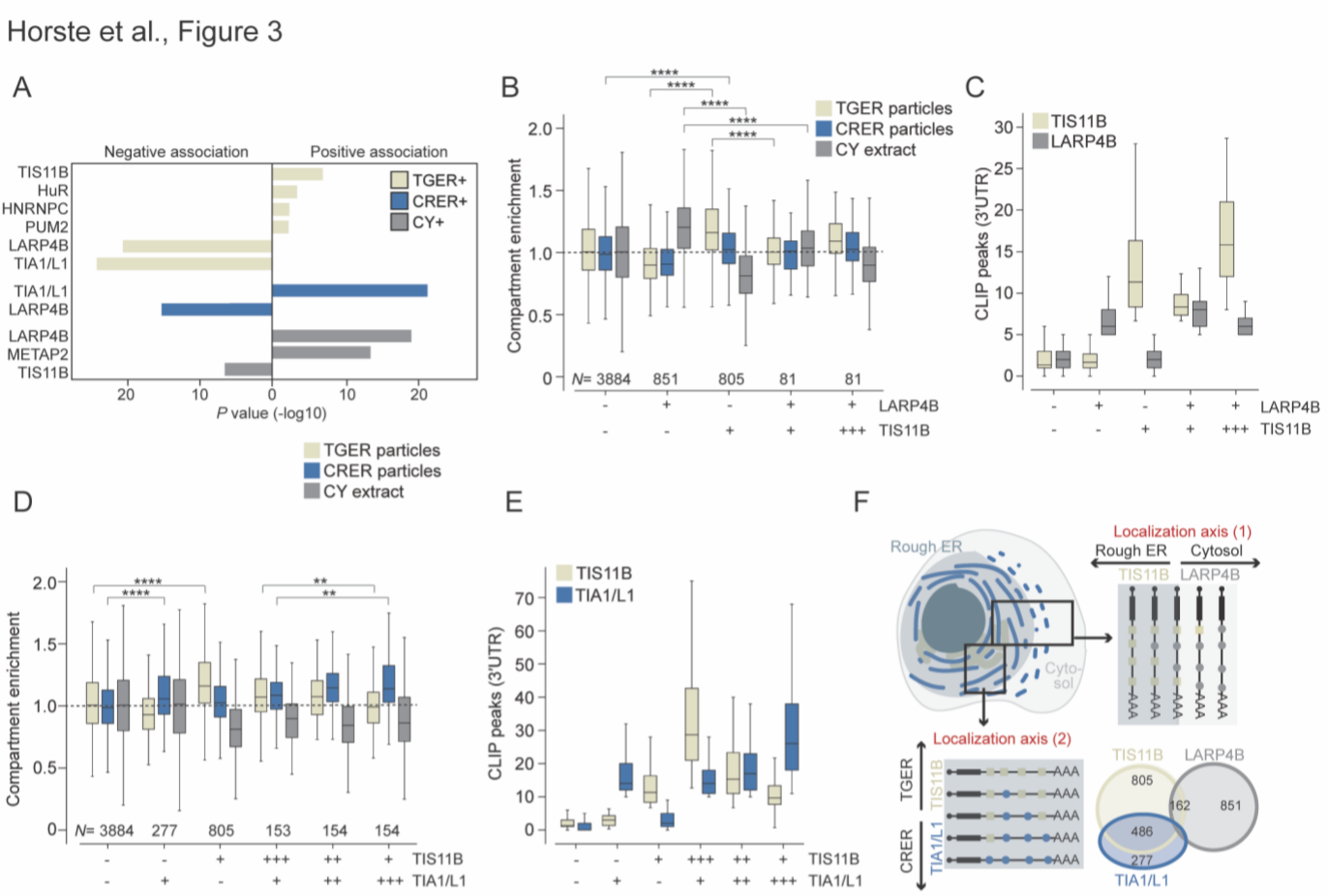

Figure 3. Subcytoplasmic mRNA localization patterns are determined by a combinatorial code of 3′UTR-bound RNA-binding proteins.

(A) 3′UTR-bound RNA-binding proteins that are positively or negatively associated with mRNAs enriched in the three subcytoplasmic compartments. Shown are the -log10 transformed *P* values obtained from logistic regression (see Table S3).

(B) Compartment-specific enrichment of mRNAs bound by LARP4B, TIS11B, both or none. Plus (+) indicates the targets of the specified RNA-binding protein, minus (-) indicates the non-targets. Mann Whitney tests were performed. CY: +/- vs -/+, *P* = 1 E-141; TGER: +/- vs -/+, *P* = 1E-111; CRER: -/- vs -/+, *P* = 4E-7; CY: +/- vs +/+, *P* = 2E-7; TGER: -/+ vs +/+, *P* = 2E-15.

(C) The number of CLIP peaks is shown for the mRNA groups from (B). LARP4B targets have 3′UTRs with more than four LARP4B peaks, TIS11B targets have 3′UTRs with more than six TIS11B peaks.

(D) As in (B), but compartment-specific enrichment of mRNAs bound by TIS11B, TIA1/L1, both or none is shown. Mann Whitney tests were performed. TGER: -/- vs +/-, *P* = 3E-57; CRER: -/- vs -/+, *P* = 2E-11; TGER: +++/+ vs +/+++, *P* = 2E-4; CRER: +++/+ vs +/+++, *P* = 0.003.

(E) The number of CLIP peaks is shown for the mRNA groups from (D). TIS11B targets have 3′UTRs with more than six TIS11B peaks, TIA1/L1 targets have 3′UTRs with more than nine TIA1/L1 peaks.

(F) Model showing two major dimensions of mRNA localization in non-polarized cells. The relative amount of 3′UTR-bound TIS11B and LARP4B determines mRNA localization between the rough ER and the cytosol, whereas the relative amount of 3′UTR-bound TIS11B and TIA1/L1 determines mRNA localization between the two rough ER domains. Shown are the numbers of mRNAs that encode non-membrane proteins that are uniquely bound or cobound by the three RNA-binding proteins.

the two RNA-binding proteins neutralizes each other's effects and the relative abundance of the two RNA-binding proteins controls the extent of ER vs cytosolic mRNA localization. For example, mRNAs bound by similar amounts of TIS11B and LARP4B lack the compartment-specific localization pattern, whereas increasing levels of TIS11B on LARP4B-bound mRNAs induce a localization pattern similar to TIS11B-only bound mRNAs, but less pronounced (Fig. 3B, 3C).

3′UTR-bound TIS11B versus TIA1/L1 discriminates mRNA localization between the two rough ER domains

Exclusive binding of TIS11B is strongly associated with mRNA localization to the TGER domain, whereas the presence of TIA1/L1 was a powerful predictor for CRER localization (Fig. 3A, 3D). Although exclusive presence of TIA1/L1 correlated with CRER localization, most TIA1/L1-positive mRNAs are cobound by TIS11B (Fig. 3D, 3E). The cobound mRNAs tend to be CRER-localized, and this tendency increases with the amount of bound TIA1/L1 (Fig. 3D, 3E).

Taken together, our data suggest that the combinatorial binding of all 3′UTR-bound RNA-binding proteins determines the localization of an mRNA to different cytoplasmic compartments in non-polarized cells (Fig. 3A, 3B, 3D, S3D, S3F). We observed two major dimensions of mRNA localization (Fig. 3F). The first axis determines mRNA localization to the rough ER or the cytosol and is controlled by the opposing forces of 3′UTR-bound TIS11B and LARP4B. The second axis describes mRNA localization between the two rough ER domains and is determined by the relative amount of 3′UTR-bound TIS11B and TIA1/L1. The observed effects on mRNA localization are additive, meaning that high levels of two RNA-binding proteins with opposing effects neutralize each other's contribution, thus preventing the establishment of a compartment-specific mRNA localization pattern. In addition, the effects are quantitative, as increasing numbers of 3′UTR binding sites occupied by specific RNA-binding proteins correlated with stronger localization effects towards their respective target compartments (Fig. 3F).

Lack of 3′UTRs in expression constructs causes default mRNA localization to the cytosol

For endogenous mRNAs, our CLIP analysis suggested that their subcytoplasmic localization pattern is established by 3′UTR-bound RNA-binding proteins. We examined if inclusion or exclusion of 3′UTRs in expression constructs will recapitulate the compartment-specific mRNA localization pattern. Expression of cDNAs derived from TGER-enriched mRNAs showed that inclusion of the 3′UTR results in mRNA enrichment in the TGER region (Fig. 4A-C, Fig. S4A). This suggests that TIS11B-bound 3′UTRs are sufficient for mRNA localization to the TGER domain as expression of the same coding regions without their corresponding 3′UTRs resulted in cytosolic localization. For cDNAs derived from cytosolic mRNAs we observed localization to the cytosol regardless of 3′UTR inclusion (Fig. S4B) and indicates default cytosolic localization in the absence of 3′UTR-bound RNA-binding proteins.

3′UTR-bound TIAL1 localizes non-membrane protein-encoding mRNAs to the ER

3′UTR-bound TIA1/L1 promotes localization of mRNAs encoding non-membrane proteins to the CRER membrane (Fig. 3A, 3D). As most of them are cobound by other RNA-binding proteins (Fig. 3D, 3E), we applied a different validation strategy and used the MS2 tethering system to mimic exclusive 3′UTR-binding of TIA1/L1 (Fig. 4D). We generated a GFP-tagged reporter mRNA that contains MS2-binding sites as 3′UTR (Bertrand et al., 1998; Berkovits and Mayr, 2015; Lee and Mayr, 2019). Coexpression of mCherry-tagged MS2 coat protein (MCP) fused to TIAL1 tethers TIAL1 to the 3′UTR of the reporter mRNA (Fig. 4D). As control, mCherry-tagged MCP was tethered to the GFP reporter mRNA.

Horste et al., Figure 4

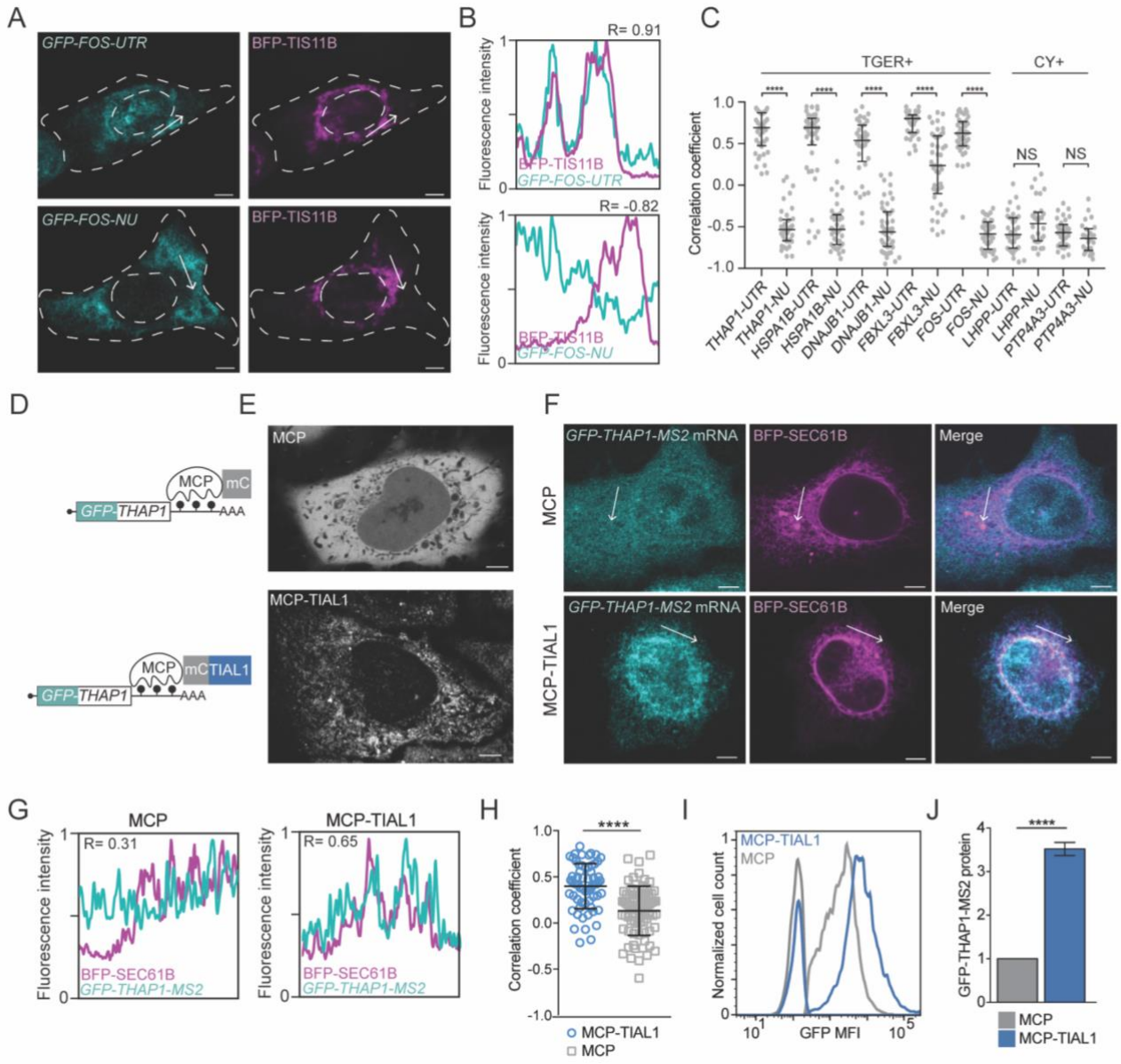

Figure 4. TIAL1-dependent mRNA localization to the rough ER strongly increases protein expression.
(A) RNA-FISH of GFP mRNA after transfection of a GFP-fused FOS coding region together with the FOS 3′UTR (FOS-UTR) or without the FOS 3′UTR (FOS-NU, no UTR) in HeLa cells (teal). Cotransfection of GFP-TIS11B to visualize TIS granules (magenta). Scale bar, 5 µm.
(B) Line diagrams showing the fluorescence intensities obtained at the position of the arrows from (A). The Pearson's correlation coefficients of the fluorescence intensities are shown.
(C) As in (A) but shown are the Pearson's correlation coefficients of additional mRNAs expressed from cDNAs either containing or lacking their corresponding 3′UTRs. Corresponding RNA-FISH images are shown in Fig. S4. Two line profiles were generated for each cell. Number of cells analyzed, *FOS-UTR N* = 14, *FOS-NU N* = 18, *THAP1-UTR N* = 15, *THAP1-NU N* = 18, *HSPA1B-UTR N* = 18, *HSPA1B-NU N* = 15, *DNAJB1-UTR N* = 13, *DNAJB1-NU N* = 18, *FBXL3-UTR N* = 12, *FBXL3-NU N* = 16, *LHPP-UTR N* = 16, *LHPP-NU N* = 12, *PTP4A3-UTR N* = 14, *PTP4A3-NU N* = 11. Mann-Whitney test, ****, $P < 0.0001$, NS, not significant; LHPP: UTR vs NU; $P = 0.1447$; PTP4A3 UTR vs NU; $P = 0.1126$.
(D) Schematic of the mRNA reporter used to validate the effect of a single 3′UTR-bound RNA-binding protein on mRNA localization and to investigate the resulting protein expression. The GFP-tagged reporter mRNA contains the THAP1 coding region and MS2 hairpins as a 3′UTR, which allow binding of the cotransfected MS2 coat protein (mCherry-tagged MCP). Fusion of TIAL1 to MCP tethers it to the 3′UTR of the reporter mRNA. mC, mCherry.

(E) Confocal live cell imaging of HeLa cells expressing mC-tagged MCP (top) or mC-tagged MCP-TIAL1 (bottom). Scale bar, 5 µm.
(F) RNA-FISH of the GFP reporter mRNA (teal) from (D) in HeLa cells coexpressing the indicated MCP-fusion construct together with BFP-SEC61B to visualize the rough ER (magenta). Representative confocal images are shown. Scale bar, 5 µm.
(G) Line profiles of the fluorescence intensities obtained from the arrows shown in (F) together with the obtained Pearson's correlation coefficients.
(H) Quantification of the Pearson's correlation coefficients between the GFP reporter mRNA and the rough ER in the experiment shown in (F). Two line profiles were generated for each cell. For MCP, $N = 26$ cells were analyzed and for MCP-TIAL1 $N = 21$ were analyzed. The horizontal line denotes the median and the error bars denote the 25th and 75th percentiles. Mann-Whitney test, ****, $P < 0.0001$.
(I) GFP protein expression of the reporter mRNA in HeLa cells measured by FACS for the samples from (D). Representative histograms are shown. The histograms on the left indicate GFP-negative cell populations.
(J) Quantification of the experiment shown in (I). Shown is the mean ± std of five independent experiments. T-test for independent samples, ****, $P = 0.0003$.

Coexpression of the reporter mRNA and MCP resulted in evenly distributed cytosolic expression of both MCP protein and reporter mRNA, due to the absence of a specific RNA-binding protein (Fig. 4E-H). In contrast, coexpression of the reporter mRNA and MCP-TIAL1 resulted in perinuclear, reticulated expression of MCP-TIAL1 with the mRNA reporter predominantly localized to the rough ER (Fig. 4E-H). Colocalization was assessed by RNA-FISH of the GFP-tagged reporter mRNA and simultaneous visualization of the rough ER through fluorescently tagged SEC61B. Using line diagrams of the fluorescence intensities, we quantified the overlap between the reporter mRNAs and the ER (Fig. 4F-H). In the presence of MCP-TIAL1, we observed higher correlation coefficients between the reporter mRNA and the ER (Fig. 4H). This result indicates that 3′UTR-bound TIAL1 causes localization of non-membrane protein encoding mRNAs to the rough ER surface.

3′UTR-bound TIAL1 increases protein expression

For endogenous mRNAs, our analysis suggested that CRER-enriched mRNAs encode proteins with the highest steady-state expression levels (Fig. 2B). Using the mRNA reporter, we investigated the contribution of TIAL1 to steady-state protein expression. We used FACS to measure GFP protein expression of the mRNA reporter with and without tethering of TIAL1 to the 3′UTR (Fig. 4D, Fig. S5A-C). We observed a 3.5-fold increase in protein expression upon 3′UTR-tethering of TIAL1 compared to tethering of MCP alone (Fig. 4I, 4J). We confirmed the TIA1/L1-dependent increase in protein expression using a second GFP reporter (Fig. S5D-F). As TIAL1 promotes translation of mRNAs on the ER membrane, it was unclear if increased protein expression was caused by TIAL1 or by a potentially unique translation environment provided by the rough ER membrane. For example, it was reported that mRNAs that encode non-membrane proteins contain 1.4-fold more ribosomes when translated on the ER membrane than when translated in the cytosol (Voigt et al., 2017).

TIAL1 cooperates with the rough ER environment to promote protein expression

To disentangle the effects of TIAL1 and the ER membrane on protein expression, we tethered the reporter mRNA directly to the ER surface by fusing MCP to SEC61B, a subunit of the translocon complex in the rough ER (Fig. 5A). MCP-SEC61B perfectly colocalized with the ER and recruited reporter mRNAs to the ER (Fig. 5B, S5G-I). However, reporter protein expression only increased by 1.25-fold compared to the tethering of MCP alone (Fig. 5B-D). We used a second ER localization reporter by fusing MCP to TRAPα, which represents a different subunit of the translocon complex and obtained a similar result. We observed an increase in protein expression by 1.5-fold when the reporter mRNA was tethered to TRAPα (Fig. S5J-M). These results suggested that the ER membrane environment has a significant but small stimulatory effect on protein expression.

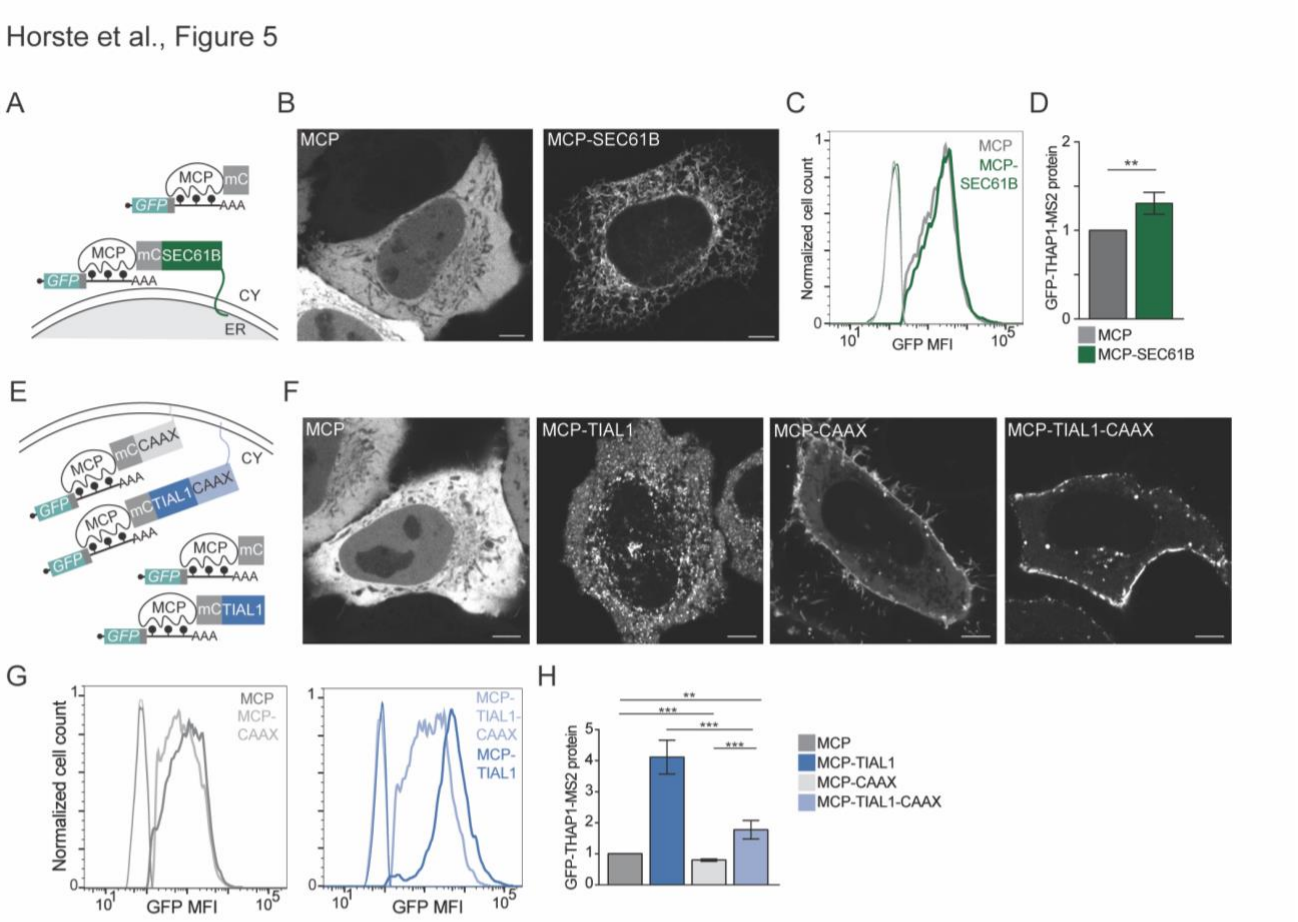

Figure 5. 3′UTR-bound TIAL1 cooperates with the rough ER membrane environment to increase protein expression.

(A) Schematic of a GFP-tagged mRNA reporter that investigates the influence of subcellular mRNA localization on protein expression. Fusion of MCP to SEC61B localizes the GFP reporter mRNA (shown as in Fig. 4D) to the rough ER membrane, whereas MCP alone localizes it to the cytosol.

(B) Confocal live cell imaging of HeLa cells expressing mC-tagged MCP (left) or mC-tagged MCP-SEC61B (right). Scale bar, 5 µm.

(C) GFP protein expression of the mRNA reporter measured by FACS in HeLa cells coexpressing the mRNA reporter together with the indicated MCP-fusion constructs. Representative histograms are shown. GFP-negative populations are plotted on the left side.

(D) Quantification of the experiment from (C). Shown is the mean ± std of four independent experiments. T-test for independent samples, **, P =0.0026.

(E) As in Fig. 4D, but addition of a prenylation signal (CAAX) localizes the TIAL1-bound GFP reporter mRNA to the plasma membrane. In the absence of CAAX, the TIAL1-bound reporter mRNA localizes to the rough ER.

(F) Confocal live cell imaging of HeLa cells expressing the indicated constructs. Scale bar, 5 µm.

(G) GFP protein expression of the mRNA reporter measured by FACS in HeLa cells coexpressing the mRNA reporter together with the indicated MCP-fusion constructs. Representative histograms are shown. GFP-negative populations are plotted on the left side.

(H) Quantification of the experiment from (G). Shown is the mean ± std of four independent experiments. T-test for independent samples, ****, $P < 0.0006$, **, $P = 0.002$.

Next, we investigated if the TIAL1-dependent increase in protein expression is intrinsic to TIAL1 or if it depends on its localization to the ER membrane. We added a CAAX motif to TIAL1 to localize the TIAL1-bound mRNA reporter to the plasma membrane instead of the ER membrane (Fig. 5E). The CAAX signal is a prenylation motif that efficiently localized MCP and MCP-TIAL1 to the plasma membrane (Fig. 5F)(Yan et al., 2016). Translation of the TIAL1-bound mRNA reporter at the plasma membrane increased protein expression by 1.8-fold (Fig. 5G, 5H). As translation of the TIAL1-bound reporter at the ER membrane resulted in two-fold higher protein expression than its translation at the plasma membrane (Fig. 5H), our result suggested that TIAL1 cooperates with the environment on the rough ER membrane to promote protein expression. As the RNA-binding proteins bound to the reporter mRNA were identical in these experiments, our results demonstrate that the subcytoplasmic location of translation controls steady-state protein expression levels by two-fold when comparing plasma and ER membranes.

The repressive effect of unassembled TIS11B on protein expression is overcome by its localization to rough ER membrane

Next, we examined if the environment on the rough ER membrane also promotes protein expression of mRNAs bound by other RNA-binding proteins, including TIS11B (Fig. 6A, 6B). In cells expressing GFP- or mCherry-TIS11B fusion constructs, about 30% form TIS granules at steady state (Fig. S6A, S6B) (Ma and Mayr, 2018). However, we noticed that addition of MCP to TIS11B fusion constructs resulted in limited TIS granule formation and predominant expression of unassembled TIS11B in the cytosol (Fig. S6A, S6B). Cytosolic, unassembled TIS11B expression, which was accomplished by tethering of MCP-TIS11B to the reporter mRNA, repressed reporter protein expression by two-fold compared to tethering of MCP alone (Fig. 6C, 6D). This result is consistent with previous reports that suggested that unassembled TIS11B represses the expression of certain cytokine mRNAs and cell cycle regulators (Stoecklin et al., 2002; Lykke-Andersen and Wagner, 2005; Galloway et al., 2016). In contrast, fusing TIS11B to MCP-SEC61B localizes TIS11B and the bound reporter mRNA to the rough ER, and this overcomes the repressive effect of unassembled TIS11B, increasing protein expression by two-fold (Fig. 6A-D). The two-fold increase in protein expression was recapitulated with a second reporter and indicates that the repressive effect on protein expression mediated by cytosolic, unassembled TIS11B is overcome by translation of the TIS11B-bound mRNA in the TGER region (Fig. 6D, Fig. S6C-E).

Taken together, we observed that 3′UTR-bound TIAL1 has a promoting effect on protein expression, whereas the binding of TIS11B is repressive. These results confirm the primary regulatory impact of RNA-binding proteins on steady-state protein expression (Fig. 5H, 6D). Moreover, protein expression is additionally regulated in a manner that is independent of the bound RNA-binding proteins but is caused by the subcytoplasmic location of translation (Fig. 5H, 6D). Our findings show that translation of mRNAs that encode non-membrane proteins on the rough ER membrane stimulates their protein expression by two-fold, regardless of the bound RNA-binding proteins (Fig. 6E).

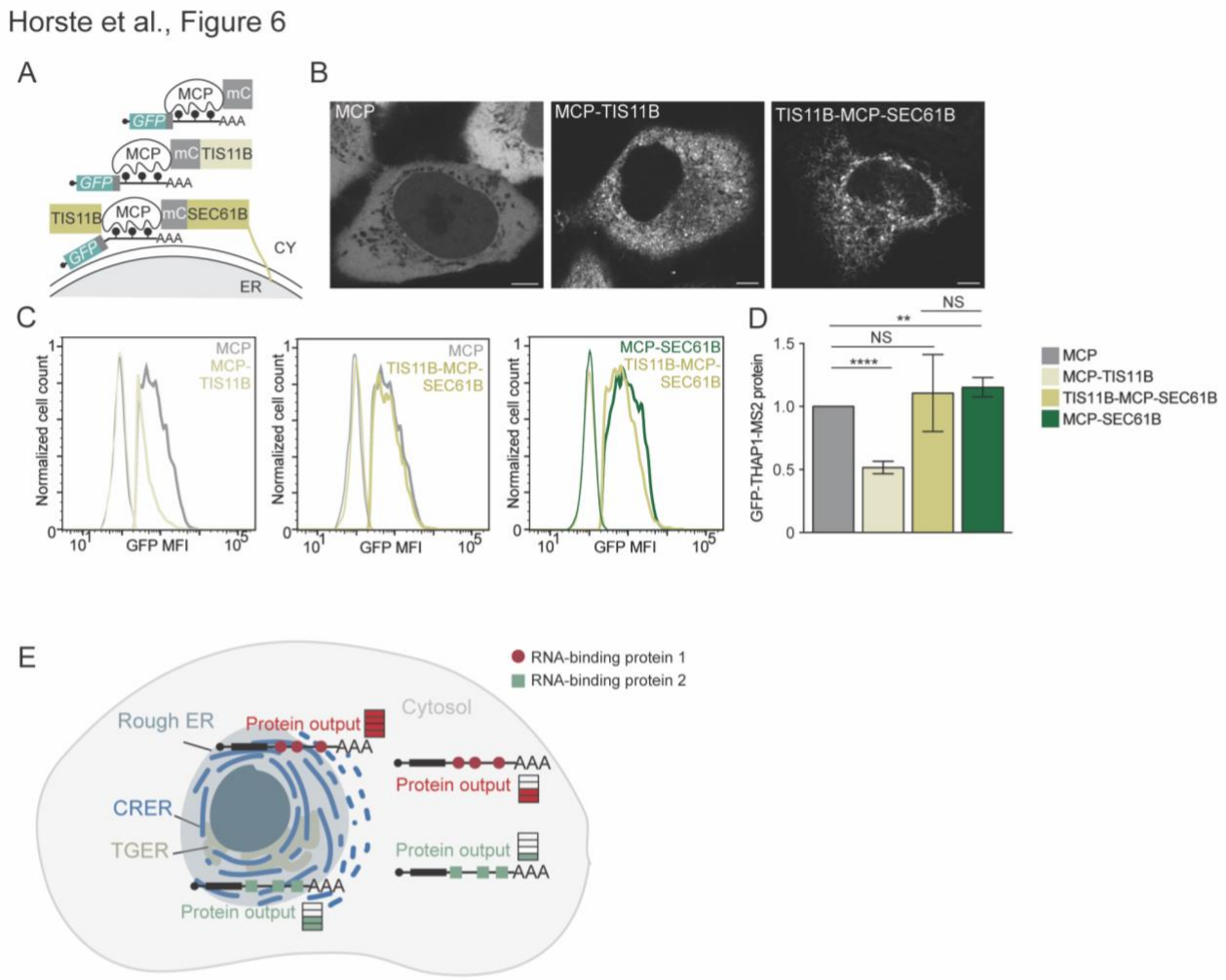

Figure 6. Relocalization of cytosolic mRNAs to the rough ER membrane increases their protein expression.
(A) Schematic of a GFP-tagged reporter mRNA bound by TIS11B that allows investigation of localization-dependent GFP protein expression. Fusion of MCP and TIS11B localizes the mRNA reporter to the cytosol, whereas the TIS11B-MCP-SEC61B fusion localizes the mRNA to the rough ER membrane.
(B) Confocal live cell imaging of HeLa cells expressing the indicated constructs (described in A). Scale bar, 5 µm.
(C) GFP protein expression of the mRNA reporter measured by FACS in HeLa cells coexpressing the mRNA reporter together with the indicated MCP-fusion constructs. Representative histograms are shown. GFP-negative populations are plotted on the left side.
(D) Quantification of the experiment from (C). Shown is the mean ± std of four independent experiments. T-test for independent samples, ****, $P < 0.0001$, **, $P = 0.03$, NS, not significant.
(E) Model for mRNA localization-dependent protein expression. Translation of mRNAs that encode non-membrane proteins on the ER membrane stimulates their protein expression by two-fold independently of the bound RNA-binding proteins. The red dots indicate RNA-binding protein 1, whereas the green squares indicate RNA-binding protein 2.

Discussion

Localized protein synthesis in non-polarized cells is best established for mRNAs that encode membrane and secretory proteins on the ER membrane (Jan et al., 2014; Fazal et al., 2019). In addition, dozens of mRNAs that encode non-membrane proteins were found by several groups to also be translated on the ER membrane (Lerner et al., 2003; Diehn et al., 2006; Chen et al., 2011; Reid and Nicchitta, 2012; Cui et al., 2012; Voigt et al., 2017). However, it was previously unknown to what extent mRNAs that encode non-membrane proteins localize to the rough ER. Using fluorescent particle sorting and digitonin extraction, we determined differential mRNA localization under steady-state cultivation conditions for two rough ER domains, such as CRER and TGER, and compared their characteristics with mRNAs enriched in the cytosol.

Widespread enrichment of mRNAs that encode non-membrane proteins at the rough ER

We confirmed that the rough ER membrane is the predominant site of protein synthesis for membrane and secretory proteins as 79% of these mRNAs (*N* = 1688) are strongly enriched there. However, we detected even more mRNAs that encode non-membrane proteins to be enriched on the rough ER (*N* = 2165), representing 31% of mRNAs encoding non-membrane proteins in our dataset (Fig. 1F). Our findings indicate that the ER membrane is a general site of active translation of both membrane and non-membrane proteins. We confirm previous reports (Lerner et al., 2003; Diehn et al., 2006; Chen et al., 2011; Reid and Nicchitta, 2012; Cui et al., 2012; Voigt et al., 2017), but we expand substantially the number of mRNAs that encode non-membrane proteins on the rough ER. As this group of mRNAs has not been characterized, we focused our analysis on these mRNAs.

Compartment-specific translation of functionally related genes

We observed that 53% of mRNAs that encode non-membrane proteins are enriched in a single cytoplasmic location. We used RNA-FISH on endogenous and transfected mRNAs to validate the results of our subcytoplasmic mRNA localization dataset and confirmed the predicted mRNA enrichment in their respective compartments (Fig. 1 and 4). One of our most striking findings was that within each cytoplasmic compartment a different group of functionally related mRNAs is translated. Moreover, the compartment-enriched mRNAs are characterized by substantially different production and degradation rates as well as expression levels of their encoded proteins (Fig. 2). These features are consistent with the compartment-enriched gene groups, indicating that the cytoplasm is strongly partitioned into different functional and regulatory compartments that are not enclosed by membranes.

For example, we observed that proteins that require to be expressed in low abundance are translated in the TGER compartment (Vaquerizas et al., 2009). We found a substantial enrichment of mRNAs that encode zinc finger proteins and transcription factors, suggesting that TGER is the preferred compartment for transcription factor translation (Fig. 2E). Moreover, transcription factors may also take advantage of other, so far unknown features of the TGER environment that may allow them to regulate protein complex assembly. This idea is based on the previous observation that membrane proteins that are translated in the TGER domain are able to establish protein complexes that cannot be formed when the proteins are translated on the ER membrane outside of TIS granules (Ma and Mayr, 2018).

In contrast, mRNAs that are the most stable and encode the most highly expressed proteins are enriched on the CRER and include helicases, cytoskeleton-bound proteins, and chromatin regulators (Fig. 2). It was previously shown that global translation is inhibited during stress, including hypoxia, but local translation on the ER is sustained. Active translation of hypoxia-induced genes was accomplished through their increased ER localization during stress

(Staudacher et al., 2015). Our findings show that the rough ER membrane is not only a privileged site of protein synthesis during stress, but additionally promotes high protein expression for a selected group of genes also in steady-state cultivation conditions.

It was previously assumed that the majority of non-membrane protein-encoding mRNAs are translated in the cytosol (Jan et al., 2014; Fazal et al., 2019). We confirm that non-membrane protein-encoding mRNAs are translated in the cytosol but show that only ~21% of these mRNAs are enriched there. The group of mRNAs overrepresented in the cytosol had the highest production and degradation rates (Fig. 2). They are enriched in proteins involved in mRNA processing and translation factors, whose abundance levels require tight control. Taken together, despite not being separated by membranes, we observed strong evidence for the functional compartmentalization of the subcytoplasmic space.

A combinatorial code of 3′UTR-bound RNA-binding proteins controls subcytoplasmic mRNA localization

According to the RNA regulon hypothesis, functionally related mRNAs are coregulated by specific RNA-binding proteins that orchestrate the different regulatory steps during their lifetime (Keene, 2007). As compartment-enriched mRNAs differed substantially in their mRNA features, we determined the RNA-binding proteins responsible for subcytoplasmic localization. In polarized cells, differential mRNA localization has been described between soma and neurites or between apical and basal compartments (Miller et al., 2002; Huttelmaier et al., 2005; Moor et al., 2017). Although HEK293T cells lack such polarity, we identified a hierarchy in subcytoplasmic mRNA localization. Differential mRNA localization between the rough ER membrane and the cytosol was largely determined by the antagonistic effects of 3′UTR-bound TIS11B and LARP4B. mRNAs bound by LARP4B are associated with cytosolic enrichment, whereas TIS11B-bound mRNAs are retained on the rough ER. If TIS11B-bound mRNAs are cobound by TIA1/L1, they tend to localize to the CRER, whereas mRNAs exclusively bound by TIS11B are enriched in the TGER domain (Fig. 3). 3′UTRs contain the majority of information on subcytoplasmic mRNA localization as in experimental settings, inclusion or omission of 3′UTRs in expression constructs controls mRNA translation in the TGER domain versus the cytosol (Fig. 4C).

Early mRNA localization studies performed in fibroblasts and neurons detected unique localization signals (Lawrence and Singer, 1986; Miller et al., 2002; Chao et al., 2010). Our study did not identify such signals, but instead, we found that 3′UTR-bound RNA-binding proteins had cumulative effects on mRNA localization. For example, we observed that increasing levels of a 3′UTR-bound RNA-binding protein enhanced its respective effect on mRNA localization, but when two RNA-binding proteins with opposing effects were bound to the same mRNA, they neutralized each other’s contribution (Fig. 3).

TIA1/L1 localizes mRNAs to the CRER and promotes protein expression

We discovered a previously undescribed role for 3′UTR-bound TIA1/L1 in mRNA localization to CRER and identified TIAL1 as a strong positive regulator of protein expression (Fig. 4J). So far, TIA1 and TIAL1 have mostly been described as regulators of pre-mRNA splicing and as translational repressors in the context of cellular stress where they assemble into stress granules (Kedersha et al., 1999; Gilks et al., 2004). However, in the absence of stress, TIA1/L1 has been reported to promote polysome association which supports our findings (Mazan-Mamczarz et al., 2006; Meyer et al., 2018).

We generated a reporter system to investigate mRNA localization-dependent regulation of protein expression. By using this new experimental system, we observed a 3.5 to 4-fold increase in protein expression caused by TIAL1 (Fig. 4J, 5H). This increase is partially achieved

by the intrinsic activity of TIAL1 but the full increase in protein expression was only accomplished through cooperative action between TIAL1 and the rough ER membrane environment (Fig. 5H). Taken together, our data suggest that non-membrane proteins that require high protein expression take advantage of the translation-promoting environment of the rough ER through recruitment of TIA1/L1.

Translation on the rough ER membrane promotes protein expression

Surprisingly, we observed that translation on the rough ER membrane also promoted protein expression for TIS11B-bound mRNAs. Unassembled TIS11B localizes to the cytosol and was previously found to repress expression of specific mRNAs (Stoecklin et al., 2002; Lykke-Andersen and Wagner, 2005; Galloway et al., 2016). We confirmed this result by showing that cytosolic unassembled TIS11B represses reporter protein expression. However, translation of a TIS11B-bound mRNA on the rough ER membrane overrode the intrinsically repressive effects of cytosolic, unassembled TIS11B (Fig. 6D).

Taken together with the results obtained from endogenous mRNAs, our findings strongly suggest that the rough ER membrane represents a privileged site for protein expression. Translation of highly abundant mRNAs on the rough ER results in highly expressed proteins, whereas translation of low-abundance mRNAs results in the generation of low-abundance proteins to ensure protein synthesis of this class of proteins which is strongly enriched in transcription factors.

The mechanism by which the rough ER membrane generates a stimulating environment for protein expression is currently unknown. It was shown previously that mRNAs are bound by more ribosomes when translated on the ER instead of the cytosol (Voigt et al., 2017). Furthermore, ER-resident enzymes may modulate the translation machinery or the 3′UTR-bound RNA-binding proteins to boost translation (Bertolotti, 2018). We speculate that the environment on the rough ER, which is generated in part by the enriched mRNAs and their bound RNA-binding proteins, may exclude repressive factors that seem to be active in the cytosol. This idea is supported by our observation that cytosolic mRNAs have the highest degradation rates (Fig. 2D).

In our dataset, cytosolically-enriched mRNAs have a higher GC-content and the lowest mRNA stability values, which is consistent with previous reports showing that GC-rich 3′UTRs are destabilizing, whereas mRNAs with AU-rich 3′UTRs are more stable (Courel et al., 2019; Litterman et al., 2019). There are currently two models that are consistent with the observed data. According to the prevailing model, mRNA stability is regulated by the mRNA-bound RNA-binding proteins (Gebauer et al., 2021), meaning the RNA-binding proteins that bind to AU-rich mRNAs would stabilize them. However, our data also support an alternative model that takes into account subcellular localization. In this model, mRNAs with AU-rich 3′UTRs use RNA-binding proteins to preferentially localize to the rough ER, a region that might be inherently protected from degradation. This latter model is supported by our reporter experiments. Although we did not measure mRNA stability rates, we observed that redirecting mRNAs to the rough ER membrane increased their protein levels independently of 3′UTR sequence, which was kept constant in the relocalization experiments (Fig. 5H, 6D).

Our study revealed a surprisingly high degree of cytoplasmic compartmentalization. This is the basis for the translation of functionally related proteins in defined environments that strongly affect mRNA stability and protein expression. Our results highlight the contribution of spatial regulation whose consequences go beyond the effects mediated by the mRNA-bound proteins. In the future, our findings may provide the basis for biotechnology applications that make use of engineered 3′UTR sequences to boost protein expression in experimental settings or to increase protein production of mRNA vaccines. However, such applications will require the

identification of short 3′UTR sequences that act as TIAL1 superbinders. Such 3′UTR sequences are expected to localize any mRNA to the CRER to stimulate protein expression.

Limitations of our study

To obtain sufficient material for TGER and CRER particle sorting, we used transfected, fluorescently labeled proteins instead of endogenous proteins. As TGER and the CRER are tightly associated (Fig. 1C), for some mRNAs that encode membrane proteins, differential mRNA localization to TGER or the CRER could not be resolved. However, despite their tight association, TGER- and CRER-enriched mRNAs that encode non-membrane proteins differed substantially in their functional gene classes and in their mRNA and protein features, suggesting that our purification method was successful.

The reporter relocalization experiments showed that the subcytoplasmic location of translation strongly influences steady-state protein expression. It is thought that both mRNA stability and translation cause this effect, but the extent by which the two regulatory mechanisms contribute to protein expression was not examined.

Acknowledgements

This work was funded by the NIH Director's Pioneer Award (DP1-GM123454), the R35GM144046 NIH grant, a grant from the Pershing Square Sohn Cancer Research Alliance, a grant from the G. Harold and Leila Y. Mathers Foundation, and the MSK Core Grant (P30 CA008748) to CM. J.U. received funding from the ERC under the European Union Horizon 2020 Research and Innovation Program (835300-RNPdynamics) and The Francis Crick Institute receives its core funding from Cancer Research UK (CC0102), the UK Medical Research Council (CC0102), and the Wellcome Trust (CC0102). An NIH F31 (CA254335-01) fellowship was awarded to E.L.H.

We thank Yevgeniy Romin and Eric Chan from the Molecular Cytology Core Facility for help with microscopy and image analysis. We thank Kathleen Daniels from the Flow Cytometry Core Facility (now Sana Biotechnologies) for help with particle sorting and Liana Boraas at Yale University School of Medicine for help with endogenous RNA-FISH. We thank Weirui Ma and Sibylle Mitschka for experimental guidance and mentorship and Alban Ordureau for analysis of the TMT mass spectrometry data. We thank Yang Luo and Sibylle Mitschka for helpful discussions and critical reading of the manuscript.

Author contributions

E.L.H. performed all experiments, except the mass spectrometry analysis whose samples were prepared by X.C. F.C.Y.L. and J.U. performed and analyzed the TIS11B iCLIP experiment. G.Z. analyzed the CLIP, and RNA-seq data with input from C.M. and integrated all datasets. M.M.F performed the logistic regression on the RNA-binding proteins. E.L.H. and C.M. conceived the project, designed the experiments, and wrote the manuscript with input from all other authors.

Declaration of Interests

The authors declare no competing interests.

Methods

Cell lines

HEK293T (human immortalized embryonic kidney cells, female origin) was purchased from ATCC. HeLa, a human cervical cancer cell line (female origin), was a gift from the lab of Jonathan S. Weissman (UCSF), provided by Calvin H. Jan. All cells were maintained at 37°C with 5% CO2 injection in Dulbecco's Modified Eagle Medium (DMEM) containing 4,500 mg/L glucose, 10% heat inactivated fetal bovine serum, 100 U/ml penicillin and 100 µg/ml streptomycin.

Constructs

Fluorescently-tagged TIS11B and SEC61B constructs. The eGFP/mCherry/BFP fusion constructs for TIS11B and SEC61B expression were described previously (Ma and Mayr, 2018). They were generated in the pcDNA3.1-puro expression vector. The TIS11B and SEC61B coding regions were PCR amplified from HeLa cDNA and inserted downstream of eGFP/mCherry/BFP using BsrGI/EcoRI or BsrGI/HindIII restriction sites, respectively.

Constructs for RNA-FISH. All coding regions were amplified from HeLa cDNA with their respective F and R primers and inserted in-frame, downstream of GFP (GFP lacking a stop codon) between BsrGI and XbaI sites into pcDNA3.1-puro-GFP vector. The corresponding 3′UTRs were amplified from HeLa genomic DNA and inserted downstream of the stop codon into the multiple cloning site using XbaI and ApaI. All primers are listed in Table S4.

Constructs to generate the mRNA localization reporter. To investigate the influence of RNA-binding proteins on mRNA localization of a GFP mRNA reporter, RNA-binding proteins were fused to MCP and tethered to a GFP mRNA reporter containing MS2 binding sites as 3′UTR (Bertrand et al., 1998; Berkovits and Mayr, 2015). To investigate mRNA localization-dependent protein expression of the GFP mRNA reporter, subcellular localization signals were fused to MCP or to MCP-RNA-binding protein fusions.

GFP mRNA reporter. To generate the GFP mRNA reporter, the GFP-BIRC3-MS2-SU (Lee and Mayr, 2019) vector was used the BIRC3 coding region was replaced with the THAP1 coding region. It was PCR amplified from the GFP-THAP1 vector using THAP1-MS2 F and THAP1-MS2 R primers and inserted between the BsrGI and AgeI sites. The SU fragment was removed with HindIII and XhoI and blunt end ligated, resulting in GFP-THAP1-MS2.

MCP-mCherry RNA-binding protein fusion constructs. To generate MCP-mCherry, the MCP coding sequence was PCR amplified from UBC NLS-HA-2XMCP-tagRFPt vector (Addgene 64541) using MCP F and MCP R primers and inserted in-frame, upstream of mCherry (mCherry lacking a start codon) between BmtI and BamHI sites in pcDNA3.1-puro-mCherry vector (Ma and Mayr, 2018). To generate MCP-mCherry-TIS11B and MCP-mCherry-TIAL1, their coding sequences were inserted in-frame, downstream of mCherry between the BsrGI and XbaI sites. The TIS11B coding sequence was amplified from pcDNA3.1-puro-GFP-TIS11B using TIS11B MCP F and TIS11B MCP R primers and the TIAL1 coding sequence was PCR amplified from pFRT_TO_FlagHA_TIAL1 (Addgene 106090) using TIAL1 MCP F and TIAL1 MCP R primers.

MCP-mCherry fusion constructs with subcellular localization signals. To generate pcDNA3.1-puro-MCP-mCherry-SEC61B, the MCP-mCherry coding sequence was cut from MCP-mCherry vector using BmtI and BsrGI and pasted in-frame, upstream of SEC61B in pcDNA3.1-mCherry-SEC61B (replacing mCherry). To generate the TIS11B-MCP-mCherry-SEC61B vector, TIS11B coding sequence was PCR amplified from pcDNA3.1-puro-GFP-TIS11B using TIS-SEC F and TIS-SEC R primers and pasted in-frame, upstream of MCP into the BmtI site in the MCP-mCherry-SEC61B vector. To generate TRAPα-MCP-mCherry, the TRAPα coding sequence

(encoded by the *SSR1* gene) was PCR amplified from HeLa cDNA using TRAPα MCP F and TRAPa MCP R and inserted in-frame, upstream of MCP in the pcDNA3.1-puro-MCP-mCherry vector.

For plasma membrane localization, the CAAX prenylation signal was added to the C-terminus of MCP-mCherry or MCP-mCherry-TIAL1. The CAAX coding sequence was purchased as a gene fragment from Azenta as described (Yan et al., 2016) and PCR amplified using TIAL1 CAAX F and CAAX R primers. It was inserted in-frame using the BsrGI and ApaI sites, located downstream of mCherry to generate pcDNA3.1-puro-MCP-mCherry-CAAX. It was inserted in-frame using EcoNI and ApaI sites to generate MCP-mCherry-TIAL1-CAAX.

SunTag constructs. To generate the SunTag-FOS vector, the FOS coding region was PCR amplified from HeLa cDNA using FOS 2F and FOS 2R primers and inserted between AgeI and BmtI sites in pcDNA4-TO-24xGCN4_v4-KIF18B-24xPP7 vector (Addgene 74928), replacing KIF18B. The FOS 3′UTR was PCR amplified from HeLa genomic DNA using FOS UTR 2F and FOS UTR 2R primers and inserted in EcoRI site downstream of the PP7 region in SunTag-FOS.

Isolation of subcytoplasmic compartments

Transfection. HEK293T cells were seeded in six 10 cm dishes at 80% confluency in antibiotic free media. After 24 hours, cells were transfected by calcium phosphate with either 3 µg mCherry-TIS11B or 3 µg GFP-SEC61B per dish.

Particle purification. 20 hours after transfection, cells were rinsed once with ice-cold PBS, scraped in 10 ml ice-cold PBS, and pelleted at 300 x g. Pellets from two plates were resuspended in 1 ml ice-cold hypotonic isolation buffer (225 mM mannitol, 75 mM sucrose, 20 mM Tris-HCl pH 7.4, 0.1 mM EDTA). Cells were lysed with 50 strokes in a 1 ml dounce-homogenizer with pestle on ice in order to shear the nuclei from the ER. Nuclei were pelleted with a two-minute spin at 600 x g. The supernatant contains the cytoplasmic membrane fraction, which was pelleted with a 15-minute spin at 7000 x g and resuspended in ice-cold PBS for fluorescent particle sorting.

Fluorescent particle sorting. Particles were sorted on a BD FACSAria III cell sorter equipped with a 70 µm nozzle. The forward-scatter threshold was decreased from 5,000 to 800 in order to visualize subcellular particles. Particles were first detected by fluorescence using the 594 nm and 488 nm excitation lasers, for mCherry-TIS11B and GFP-SEC61B respectively, and 405 nm excitation laser for DAPI. A sorting gate was drawn on particles that were either mCherry-positive or GFP-positive, but DAPI-negative, to exclude any remaining nuclei. Sorting was performed in purity mode with an average speed of 150 particles/second. Particles were sorted directly into 1 ml of TRIzol solution in Eppendorf tubes, holding 180,000 particles per tube. RNA extraction was performed for each tube separately and total RNA for each sample was combined for library preparation. Two biological replicates for each particle prep were sequenced. For each replicate, about 1.5 million TIS11B granule particles and 2.0 million ER particles were collected.

Cytosol extraction. The cytosol was extracted as previously described (Liu and Fagotto, 2011). HEK293T cells were plated in a six-well plate at 80% confluency. After 24 hours, cells were rinsed once in the dish with ice-cold PBS. After aspirating PBS, 300 µl ice-cold digitonin solution (40 µg/ml digitonin, 150 mM NaCl, 20 mM HEPES pH 7.4, 0.2 mM EDTA, 2 mM DTT, 2 mM MgCl2) was added and incubated on a shaker at 4°C for ten minutes. After incubation, the digitonin-derived cytosolic extract was pipetted from the plate and spun at 20,000 x g for one minute to pellet any floating cells. 200 µl of cytosolic extract was added to 1 ml TRIzol solution for RNA extraction.

RNA-seq library preparation

RiboGreen RNA Reagent (ThermoFisher) was used for RNA quantification and quality control was performed by Agilent BioAnalyzer. 50-500 ng of total RNA underwent polyA selection and TruSeq library preparation according to instructions provided by Illumina (TruSeq Stranded mRNA LT Kit, catalog # RS-122-2102), with eight cycles of PCR. Samples were barcoded and run on a HiSeq 4000 in a PE50 run, using the HiSeq 3000/4000 SBS Kit (Illumina). An average of 27 million paired reads was generated per sample.

Western Blotting

For whole cell lysate preparation, cells were trypsinized and washed twice with PBS and lysed in 2x Laemmli Sample buffer (Alfa Aesar, J61337). For cytosolic lysate, cytosol was extracted with digitonin as described above and one volume of 2x Laemmli Sample buffer was added. Laemmli lysates were boiled for 10 min at 95°C. Samples were subjected to SDS-PAGE on NuPAGE 4%–12% Bis-Tris gradient protein gel (Invitrogen). Imaging was captured on the Odyssey DLx imaging system (Li-Cor). The antibodies used are listed in the Key Resources Table.

TIS11B iCLIP

Transfection. HEK293T cells were seeded in 10 cm dishes at 80% confluency in antibiotic free media. After 24 hours, cells were transfected by calcium phosphate with either 3 µg GFP-TIS11B or 1.5 µg GFP-only per dish.

Sample preparation. 20 hours after transfection, cells were rinsed once with ice-cold PBS and 6 ml of fresh PBS was added to each plate before crosslinking. Cells were irradiated once with 150 mJ/cm^2 in a Spectroline UV Crosslinker at 254 nm. Irradiated cells were scraped into Eppendorf tubes, spun at 500 x g for one minute, and snap-frozen. Crosslinked cell pellets were lysed in iCLIP lysis buffer (50 mM Tris-HCl pH 7.4, 100 mM NaCl, 1% Igepal CA-630 (Sigma I8896), 0.1% SDS, 0.5% sodium deoxycholate), sonicated with the Bioruptor Pico for 10 cycles 30 seconds ON/30 seconds OFF, and supplemented with 0.5 U of RNase I per 1 mg/ml lysate for RNA fragmentation. Lysates were pre-cleared by centrifugation at 20,000 x g at 4°C. A mix of Protein A/G Dynabeads (50 µl of each per sample, Life Technologies) were coupled to 10 µg of rabbit anti-GFP antibody (Abcam ab290). TIS11B protein-RNA complexes were immunoprecipitated from 1 ml of crosslinked lysate and washed with high salt and PNK buffer (NEB). RNA was repaired by 3′ dephosphorylation and ligated to L3-IR adaptor on beads (Zarnegar et al., 2016). Excess adaptor was removed by incubation with 5′ deadenylase and the exonuclease RecJf (NEB). TIS11B protein-RNA complexes were eluted from the beads by heating at 70°C for one minute. The complexes were then visualized via the infrared-labeled adaptor, purified with SDS-PAGE, and transferred to nitrocellulose membrane. cDNA was synthesized with Superscript IV Reverse Transcriptase (Life Technologies) and circularized by CircLigase II. Circularized cDNA was purified with AmPURE bead-based purification (A63880, Beckman Coulter), amplified by PCR and sequenced by Novaseq.

RNA-FISH

Single molecule RNA-FISH for endogenous mRNAs. Probe design. Primary probes were designed using the ProbeDealer package in MATLAB (Hu et al., 2020). Each primary probe contains 30 transcript-targeting nucleotides preceded by 20 common nucleotides that are complementary to the secondary probe. At least 30 probes were designed for each transcript, purchased in a pool from IDT. The secondary probes are 5′ conjugated to AlexaFluor 633 and were purchased from IDT.

Transfection. Prior to cell seeding, 35 mm glass cover slips were sterilized with ethanol then incubated in 1 µg/ml fibronectin in PBS at room temperature for one hour. Cover slips were

rinsed in PBS and HeLa cells were seeded at 100,000 per coverslip. 24 hours after seeding, cells were transfected with 500 ng GFP-TIS11B using Lipofectamine 3000 (Invitrogen).

Sample preparation. 20 hours after transfection, cells were rinsed once with PBS then fixed in 4% paraformaldehyde for 10 minutes at room temperature. All steps were performed at room temperature if not otherwise noted. Cells were rinsed twice with PBS and permeabilized with 0.5% Triton-X solution for 10 minutes. Cells were rinsed twice with PBS and incubated for five minutes in pre-hybridization buffer (2xSSC, 50% formamide). Cells were incubated in primary probe hybridization solution (40 µM primary probe, 2xSSC, 50% formamide, 10% dextran sulfate (Sigma), 200 µg/ml yeast tRNA (Sigma), 1:100 Murine RNase Inhibitor (NEB)), for at least 15 hours at 37°C. To remove excess or unbound primary probes, cells were then rinsed twice in 2xSSC + 0.1% Tween for 15 minutes at 60°C then once more for 15 minutes at room temperature. Cells were incubated in secondary probe solution (4 nM secondary probe, 2xSSC, 50% ethylene carbonate, 1:100 Murine RNase Inhibitor) for 30 minutes in the dark. Secondary probes were rinsed twice in 50% ethylene carbonate, 2xSSC solution for five minutes then mounted with Prolong Diamond mounting solution (Invitrogen). For both endogenous and GFP-fusion constructs, RNA-FISH images were captured using confocal ZEISS LSM 880 with Airyscan super-resolution mode.

Cytosol extraction. To visualize and validate cytosolic versus ER-associated endogenous mRNAs, HeLa cells were seeded as described above, then incubated in 2 ml digitonin solution described above (40 µg/ml digitonin, 150 mM NaCl, 20 mM HEPES pH 7.4, 0.2 mM EDTA, 2 mM DTT, 2 mM MgCl2) for 10 min at 4°C. Digitonin solution was removed, coverslips were rinsed with 2 ml PBS, and RNA-FISH was performed as described above.

Line profile analysis. To quantify colocalization of two fluorescence signals (mRNA vs TGER or mRNA vs ER), line profiles were generated with FIJI (ImageJ). For each cell, 2-4 straight lines were drawn to cross TGER (or the ER) in different directions, indicated by the white arrows shown in the figures. Fluorescence signal along the straight line of TGER (or ER) and the examined mRNA was calculated for each channel using the plot profile tool in FIJI. The values of the Pearson's correlation coefficient r were calculated using Excel. Perfect correlation of protein-mRNA is indicated by r = 1, perfect exclusion is indicated by r = -1, and random distribution is indicated by r = 0.

Enrichment analysis of endogenous mRNAs. Enrichment of endogenous mRNAs in TGER was determined using FIJI. The total area of the cell and the total area occupied by TIS granules was calculated for each cell. A mask was created from the GFP-TIS11B signal and the mask area was divided by the total cell area to generate the granule area fraction. The total number of transcripts per cell (number of foci) was quantified. This value was multiplied by the granule area fraction to yield the number of transcripts expected to be present in TIS granules by chance. The observed number of transcripts in the TIS granule area was then divided by the expected value to obtain the enrichment fold-change. The fold-change values were log2-transformed. An enrichment score of 0 indicates 'no enrichment' and is observed when the observed and expected numbers of transcripts in TIS granules are the same. A positive enrichment score indicates that there are more transcripts localized to TIS granules than one would expect by chance and a negative enrichment score indicates fewer transcripts in TIS granules than one would expect by chance.

RNA-FISH after transfection of constructs. RNA-FISH experiments probing for GFP-fusion constructs were performed as described previously (Ma and Mayr, 2018). Stellaris FISH probes for eGFP with Quasar 670 Dye were used.

Confocal microscopy

Confocal imaging was performed using ZEISS LSM 880 with Airyscan super-resolution mode. A Plan-Apochromat 63x/1.4 Oil objective (Zeiss) was used. For live cell imaging, cells were incubated with a LiveCell imaging chamber (Zeiss) at 37°C and 5% CO2 and imaged in cell culture media. Excitations were performed sequentially using 405, 488, 594 or 633 nm laser wavelength and imaging conditions were experimentally optimized to minimize bleed-through. Images were prepared with FIJI (ImageJ) software.

TMT mass spectrometry

To obtain protein expression levels, TMT mass spectrometry analysis was performed on HEK293T cells cultivated in steady-state conditions. Cells were trypsinized and washed three times with ice-cold PBS. Pelleted cells were snap-frozen in liquid nitrogen. Cell pellets were lysed with 200 µl buffer containing 8 M urea and 200 mM EPPS (pH at 8.5) with protease inhibitor (Roche) and phosphatase inhibitor cocktails 2 and 3 (Sigma). Benzonase (Millipore) was added to a concentration of 50 µg/ml and incubated at room temperature for 15 min followed by water bath sonication. Samples were centrifuged at 14,000 g at 4°C for 10 min, and supernatant extracted. The Pierce bicinchoninic acid (BCA) protein concentration assay was used to determine protein concentration. Protein disulfide bonds were reduced with 5 mM tris (2-carboxyethyl) phosphine at room temperature for 15 min, and alkylated with 10 mM iodoacetamide at room temperature for 30 min in the dark. The reaction was quenched with 10 mM dithiothreitol at room temperature for 15 min. Aliquots of 100 µg were taken for each sample and diluted to 100 µl with lysis buffer. Samples were subject to chloroform/methanol precipitation as previously described (Navarrete-Perea et al., 2018). Pellets were reconstituted in 200 mM EPPS buffer and digested with Lys-C (1:50 enzyme-to-protein ratio) and trypsin (1:50 enzyme-to-protein ratio), and digested at 37°C overnight.

Peptides were TMT-labeled as described (Navarrete-Perea et al., 2018). Briefly, peptides were TMT-tagged by the addition of anhydrous ACN and TMTPro reagents (16plex) for each respective sample and incubated for 1 hour at room temperature. A ratio check was performed by taking a 1 µl aliquot from each sample and desalted by StageTip method (Rappsilber et al., 2007). TMT tags were then quenched with hydroxylamine to a final concentration of 0.3% for 15 min at room temperature. Samples were pooled 1:1 based on the ratio check and vacuum-centrifuged to dryness. Dried peptides were reconstituted in 1 ml of 3% ACN/1% TFA, desalted using a 100 mg tC18 SepPak (Waters), and vacuum-centrifuged overnight.

Peptides were centrifuged to dryness and reconstituted in 1 ml of 1% ACN/25mM ABC. Peptides were fractionated into 48 fractions. Briefly, an Ultimate 3000 HPLC (Dionex) coupled to an Ultimate 3000 Fraction Collector using a Waters XBridge BEH130 C18 column (3.5 um 4.6 x 250 mm) was operated at 1 ml/min. Buffer A, B, and C consisted of 100% water, 100% ACN, and 25mM ABC, respectively. The fractionation gradient operated as follows: 1% B to 5% B in 1 min, 5% B to 35% B in 61 min, 35% B to 60% B in 5 min, 60% B to 70% B in 3 min, 70% B to 1% B in 10 min, with 10% C the entire gradient to maintain pH. The 48 fractions were then concatenated to 12 fractions, (i.e. fractions 1, 13, 25, 37 were pooled, followed by fractions 2, 14, 26, 38, etc.) so that every 12th fraction was used to pool. Pooled fractions were vacuum-centrifuged and then reconstituted in 1% ACN/0.1% FA for LC-MS/MS.

Fractions were analyzed by LC-MS/MS using a NanoAcquity (Waters) with a 50 cm (inner diameter 75 µm) EASY-Spray Column (PepMap RSLC, C18, 2 µm, 100 Å) heated to 60°C coupled to an Orbitrap Eclipse Tribrid Mass Spectrometer (Thermo Fisher Scientific). Peptides were separated by direct injection at a flow rate of 300 nl/min using a gradient of 5 to 30% acetonitrile (0.1% FA) in water (0.1% FA) over 3 hours and then to 50% ACN in 30 min and analyzed by SPS-MS3. MS1 scans were acquired over a range of m/z 375-1500, 120K resolution, AGC target (standard), and maximum IT of 50 ms. MS2 scans were acquired on

MS1 scans of charge 2-7 using isolation of 0.5 m/z, collision-induced dissociation with activation of 32%, turbo scan, and max IT of 120 ms. MS3 scans were acquired using specific precursor selection (SPS) of 10 isolation notches, m/z range 110-1000, 50K resolution, AGC target (custom, 200%), HCD activation of 65%, max IT of 150 ms, and dynamic exclusion of 60 s.

Visualization of translation in TGER

The SunTag system was used to visualize mRNA translation in the cytosol and the TGER domain. Stable expression of td-PP7-3xmCherry (Addgene 74926) and scFv-GCN4-sfGFP (Addgene 60907) was achieved by generating virus in HEK293T cells and transducing HeLa cells. Cells were seeded on 3.5 cm glass bottom dishes (Cellvis, D35-20-1-N). 20 hours later, cells were transfected with either the SunTag vector expressing KIF18B (Addgene 74928) or SunTag-FOS-UTR. At 15 hours post transfection, cells were treated with 100 ng/ml doxycycline for one hour to induce SunTag expression. Confocal imaging was performed as described above. Colocalization of puncta was quantified using FIJI.

mRNA localization-dependent GFP protein expression

Transfection. HeLa cells were seeded in 12-well plates at 80% confluency and transfected with 250 ng GFP-THAP1-MS2 and 250 ng of the MCP-mCherry fusion constructs indicated in the figure (Lipofectamine 3000, Invitrogen). When indicated, GFP-THAP1 or GFP-BIRC3-MS2-SU was used instead of GFP-THAP1-MS2. At 13-15 hours post transfection, cells were analyzed by FACS. For RNA-FISH experiments, cells were seeded at 80% confluency in 4-well slide chambers (Millipore Sigma) and cotransfected with 75 ng GFP-THAP1-MS2, 100 ng BFP-SEC61B, and 75 ng of the indicated MCP-mCherry fusion constructs.

FACS analysis to measure GFP protein expression. Cells were trypsinized, washed once in complete media, then resuspended in FACS buffer (PBS plus 1% FCS). At least 5,000 cells were measured on a BD LSR-Fortessa Cell Analyzer and FACS data were analyzed using FlowJo software. GFP protein expression corresponds to GFP mean fluorescence intensity (MFI). To determine the effect of MCP-tethered RNA-binding proteins on protein output of the GFP reporter mRNA, only cells that were successfully cotransfected with both the MCP-mCherry fusion and the GFP reporter constructs were analyzed. To do so, the double-positive cells (mCherry+/GFP+) were gated, and all single positive and unstained cells were excluded from the analysis. The reported GFP MFI was calculated from the double-positive cells. Untransfected cells were used to draw the gates for mCherry+ or GFP+ cells.

Data analysis

RNA-seq of subcytoplasmic fractions

RNA-seq. Raw reads were processed by trimmomatic (version: 0.39) to trim low-quality ends (average quality per base < 15, 4 bp window) and adapters (Bolger et al., 2014). Trimmed reads were mapped to the human genome (hg19) using hisat2 (version: 2.1.0) (Kim et al., 2019). Reads mapped to each gene were counted using featureCounts (version: 1.6.4) (Liao et al., 2014). RPKM values for each gene were calculated using a custom Perl script. The mean RPKM values of all biological replicates were calculated and used for downstream analyses. Only protein-coding genes were analyzed. A gene is considered expressed if the RPKM value is 3 or greater.

Classification of membrane/secretory proteins versus non-membrane proteins. All expressed genes were separated into mRNAs that encode membrane/secretory proteins or non-membrane proteins. Information on the presence of transmembrane domains or a signal sequence was obtained from uniprot. If a protein contains a signal sequence but not a transmembrane domain,

it is considered as secretory protein. All proteins with transmembrane domains are considered membrane proteins and all remaining proteins are classified as non-membrane proteins. Among the 9155 mRNAs expressed in HEK293T cells, 2140 were classified as membrane/secretory proteins, whereas 7015 were classified as non-membrane proteins (Table S1).

Compartment-specific partition coefficients. The sum of RPKM values obtained from TGER particles, CRER particles, and the cytosol was considered as total cytoplasmic mRNA expression. For each gene, the fraction of transcripts that localize to each of the three compartments was calculated by dividing its compartment-specific RPKM value by the total cytoplasmic mRNA expression (Fig. S1E).

Compartment-specific enrichment of mRNAs that encode membrane/secretory proteins. We considered an mRNA to be CRER-enriched if the ratio of partition coefficients (CRER/TGER) was greater than 1.25 and classified it as TGER-enriched if it was smaller than 0.8. The median partition coefficient of membrane/secretory mRNAs in the cytosol was 0.09. If the cytosolic partition coefficient of an mRNA was greater than 0.36, it was considered enriched in the cytosol. If the CRER and TGER-specific partition coefficients were similar and the cytosolic partition coefficient was smaller than 0.18, the mRNA was assigned to the CRER, whereas it was considered not localized if the cytosolic partition coefficient was smaller than 0.18 (Fig. S1F).

Compartment-specific enrichment of mRNAs that encode non-membrane proteins. For all mRNAs that encode non-membrane proteins, the median of the partition coefficients for each compartment were calculated. For TGER particles the median was 0.32, for CRER particles, it was 0.30 and for the cytosol, the median was 0.34. We obtained the normalized partition coefficients by dividing the compartment-specific partition coefficients by each median (Fig. 1E). An mRNA was considered enriched in a specific compartment if its normalized compartment-specific partition coefficient was greater or equal to 1.25. If the enrichment was observed in two compartments, the mRNA was considered not localized. However, when the difference between the two compartments was greater than 0.15, the mRNA was assigned to the compartment with the higher value. This strategy resulted in 1246 mRNAs considered to be TGER-enriched, 919 mRNAs to be ER-enriched, and 1481 mRNAs to be enriched in the cytosol. The remaining 3368 mRNAs are either enriched in two compartments or do not have a compartment-specific mRNA localization pattern.

mRNA and protein features of the localized mRNAs

RPKM values of mRNAs were obtained from RNA-seq data of unfractionated HEK293T cells and were determined for the compartment-enriched mRNAs. Pro-seq and RNA-seq from HEK293 cells were obtained from GEO (GSE140365: PRO-seq; GSE142895: RNA-seq) (Patel et al., 2020). Raw reads were processed by trimmomatic (version: 0.39) to trim low-quality ends (average quality per base < 15, 4 bp window) and adapters (Bolger et al., 2014). Trimmed reads were mapped to the human genome (hg19) using hisat2 (version: 2.1.0) (Kim et al., 2019). Reads mapped to each gene were counted by featureCounts (version: 1.6.4) (Liao et al., 2014). To estimate mRNA stability rates, log2-normalized counts of Pro-seq data were divided by the log2-normalized RNA-seq data, as described previously (Blumberg et al., 2021). 3′UTR length of each mRNA was obtained from Ref-seq. The longest 3′UTR isoform of each gene is reported. AU-content in 3′UTRs is the sum of all adenosines and uridines in annotated 3′UTRs divided by the total number of nucleotides in 3′UTRs. The number of AUUUA (AU-rich element) in 3′UTRs were counted. Protein length was obtained from uniprot.

Protein expression

Protein expression was obtained from TMT-based quantitative mass spectrometry analysis of unfractionated HEK293T cells. Precursor protein abundance was calculated for each protein and scaled to the TMT abundance for each channel. Relative abundance was then calculated by averaging biological replicates.

CLIP data analysis

iCLIP analysis of TIS11B in HEK293T cells. Raw fastq files were demultiplexed using the iCount python package (https://icount.readthedocs.io). 5′ and 3′ adapters were trimmed by Cutadapt (Martin, 2011). Trimmed reads were mapped to human genome using STAR and reads mapping to tRNA/rRNA were discarded (Dobin et al., 2013). Crosslink sites were called from bam files using the “xlsites” function of iCount. CLIP-seq analysis was carried out on the iMaps platform (https://imaps.genialis.com/iclip), where peak calling was performed by analysing cDNA counts at crosslink sites using Paraclu (Frith et al., 2008). Motif analysis was carried out using HOMER software. Enrichment was calculated within the genomic coordinates of a total of 57,714 TIS11B CLIP peaks found in 3′UTRs. Total peaks: 190,920; peaks in 3′UTRs: 57,714.

POSTAR3 CLIP data. CLIP data on 168 RNA-binding proteins were downloaded from Postar3 (Zhao et al., 2021) and peak counts that overlapped with annotated 3′UTRs from Ref-seq in all mRNAs that encode non-membrane proteins were recorded. For each RNA-binding protein, the median number of 3′UTRs CLIP peaks was calculated and all 3′UTRs with peaks counts greater than the median were considered as targets. Based on the fraction of mRNAs that are considered compartment-specific (TG: 17.8%; ER 13.1%; CY: 21.1%; not localized: 48.0%), we determined the expected number of target genes for each compartment. If the observed number of targets divided by the expected number of targets in a compartment was greater than 1.5, the RNA-binding protein was added to our short-list (Table S3). As TIS11B and TIA1/L1 are known to bind to AU-rich sequences, we added the processed PAR-CLIP data of the LARP4B RNA-binding protein as it was reported to bind to AU-rich elements (Küspert et al., 2015).

Logistic regression. The R package `nnet` (v7.3-17) was used to fit a logistic regression model using the CLIP peak counts from the RNA-binding proteins on the short list (N = 25) to predict the subcytoplasmic mRNA localization of non-membrane proteins. Covariates with missing values were imputed as zeros. All covariates were first `sqrt` transformed and then standardized. The ‘not localized’ category was used as the base level. The R package `broom` (v0.8.0) was used to compute t-test statistics for the model coefficients. The code is available on github (github.com/Mayrlab/tiger-seq).

Confirmation of the logistic regression. The logistic regression analysis identified TIS11B, TIA1/L1, and LARP4B as the RNA-binding proteins with the strongest influence on subcytoplasmic mRNA localization. To validate the contribution of each individual RNA-binding protein, we used more stringent criteria to determine their targets. Among all mRNAs that encode non-membrane proteins with at least one CLIP peak in the 3′UTR, we considered the top third of mRNAs as targets of each RNA-binding protein (TIS11B: 1781 targets; TIA1/L1: 1313 targets; LARP4B: 1621 targets; METAP2: 256 targets; HuR: 1124 targets; PUM2: 427 targets; HNRNPC: 232 targets).

Intersection of membrane/secretory mRNAs with previous datasets. The mRNAs that are coexpressed in our RNA-seq dataset (N = 9155 mRNAs) and the ER membrane-localized mRNAs from the APEX-seq dataset (N = 1045) were determined (Fazal et al., 2019). The overlapping 845 mRNAs were intersected with the mRNAs that encode membrane/secretory proteins found to be enriched on the ER in our analysis (N = 1476). We detected 673 mRNAs which correspond to 80% of all APEX-seq mRNAs that are considered to be ER membrane-enriched. The universe used to test for enrichment were all mRNAs that encode non-membrane proteins (N = 2140). A similar analysis was performed for the fractionation dataset from Reid

(2012) (Reid and Nicchitta, 2012). Among the 385 coexpressed mRNAs that are enriched on the ER according to Reid, we detected 308 in our ER-enriched fraction when focusing on membrane/secretory protein encoding mRNAs. This group represents 80% of all ER-enriched mRNAs detected by Reid.

Gene ontology analysis

Gene ontology (GO) analysis was performed using DAVID (Huang da et al., 2009).

Further statistical analysis

Statistical parameters are reported in the figures and figure legends, including the definitions and exact values of *N* and experimental measures (mean ± std or boxplots depicting median, 25^{th} and 75^{th} percentile (boxes) and 5% and 95% confidence intervals (error bars). Feature comparison across more than two groups was performed using a Kruskal-Wallis test, pair-wise comparisons were performed using a two-sided Mann-Whitney test. Enrichment was determined using a X^2 test. The *P* value was calculated using a two-sided Fisher's exact test. When indicated, a two-sided t-test with assumption of equal variance was applied. Statistical significance is indicated by asterisks *, $P < 0.05$, **, $P < 0.01$, ***, $P < 0.001$, ****, $P < 0.0001$.

Data and code availability

The mass spectrometry data are reported in Table S1. The RNA-seq samples obtained from the subcytoplasmic fractionation and the TIS11B iCLIP data obtained from HEK293T cells are available at GEO (Accession number: GSE215770). The code for logistic regression is available on github.

References

Banani, S.F., Lee, H.O., Hyman, A.A., and Rosen, M.K. (2017). Biomolecular condensates: organizers of cellular biochemistry. Nature reviews Molecular cell biology *18*, 285-298.

Berkovits, B.D., and Mayr, C. (2015). Alternative 3' UTRs act as scaffolds to regulate membrane protein localization. Nature *522*, 363-367.

Bertolotti, A. (2018). The split protein phosphatase system. The Biochemical journal *475*, 3707-3723.

Bertrand, E., Chartrand, P., Schaefer, M., Shenoy, S.M., Singer, R.H., and Long, R.M. (1998). Localization of ASH1 mRNA particles in living yeast. Mol Cell *2*, 437-445.

Biever, A., Donlin-Asp, P.G., and Schuman, E.M. (2019). Local translation in neuronal processes. Current opinion in neurobiology *57*, 141-148.

Blumberg, A., Zhao, Y., Huang, Y.-F., Dukler, N., Rice, E.J., Chivu, A.G., Krumholz, K., Danko, C.G., and Siepel, A. (2021). Characterizing RNA stability genome-wide through combined analysis of PRO-seq and RNA-seq data. BMC biology *19*, 30.

Bolger, A.M., Lohse, M., and Usadel, B. (2014). Trimmomatic: a flexible trimmer for Illumina sequence data. Bioinformatics *30*, 2114-2120.

Boraas, L., Hu, M., Thornton, L., Vejnar, C.E., Zhen, G., Giraldez, A.J., Mayr, C., Wang, S., and Nicoli, S. (2021). Non-coding function for mRNAs in Focal Adhesion Architecture and Mechanotransduction. bioRxiv, 2021.2010.2004.463097.

Buxbaum, A.R., Haimovich, G., and Singer, R.H. (2015). In the right place at the right time: visualizing and understanding mRNA localization. Nature reviews Molecular cell biology *16*, 95-109.

Chao, J.A., Patskovsky, Y., Patel, V., Levy, M., Almo, S.C., and Singer, R.H. (2010). ZBP1 recognition of beta-actin zipcode induces RNA looping. Genes Dev *24*, 148-158.

Chen, Q., Jagannathan, S., Reid, D.W., Zheng, T., and Nicchitta, C.V. (2011). Hierarchical regulation of mRNA partitioning between the cytoplasm and the endoplasmic reticulum of mammalian cells. Molecular biology of the cell *22*, 2646-2658.

Courel, M., Clément, Y., Bossevain, C., Foretek, D., Vidal Cruchez, O., Yi, Z., Bénard, M., Benassy, M.N., Kress, M., Vindry, C.*, et al.* (2019). GC content shapes mRNA storage and decay in human cells. eLife *8*.

Cui, X.A., Zhang, H., and Palazzo, A.F. (2012). p180 promotes the ribosome-independent localization of a subset of mRNA to the endoplasmic reticulum. PLoS Biol *10*, e1001336.

Diehn, M., Bhattacharya, R., Botstein, D., and Brown, P.O. (2006). Genome-scale identification of membrane-associated human mRNAs. PLoS Genet *2*, e11.

Dobin, A., Davis, C.A., Schlesinger, F., Drenkow, J., Zaleski, C., Jha, S., Batut, P., Chaisson, M., and Gingeras, T.R. (2013). STAR: ultrafast universal RNA-seq aligner. Bioinformatics *29*, 15-21.

Fazal, F.M., Han, S., Parker, K.R., Kaewsapsak, P., Xu, J., Boettiger, A.N., Chang, H.Y., and Ting, A.Y. (2019). Atlas of Subcellular RNA Localization Revealed by APEX-Seq. Cell *178*, 473-490.e426.

Frith, M.C., Valen, E., Krogh, A., Hayashizaki, Y., Carninci, P., and Sandelin, A. (2008). A code for transcription initiation in mammalian genomes. Genome Res *18*, 1-12.

Galloway, A., Saveliev, A., Lukasiak, S., Hodson, D.J., Bolland, D., Balmanno, K., Ahlfors, H., Monzon-Casanova, E., Mannurita, S.C., Bell, L.S.*, et al.* (2016). RNA-binding proteins ZFP36L1 and ZFP36L2 promote cell quiescence. Science *352*, 453-459.

Gebauer, F., Schwarzl, T., Valcárcel, J., and Hentze, M.W. (2021). RNA-binding proteins in human genetic disease. Nature reviews Genetics *22*, 185-198.

Gilks, N., Kedersha, N., Ayodele, M., Shen, L., Stoecklin, G., Dember, L.M., and Anderson, P. (2004). Stress granule assembly is mediated by prion-like aggregation of TIA-1. Molecular biology of the cell *15*, 5383-5398.

Glock, C., Biever, A., Tushev, G., Nassim-Assir, B., Kao, A., Bartnik, I., Tom Dieck, S., and Schuman, E.M. (2021). The translatome of neuronal cell bodies, dendrites, and axons. Proc Natl Acad Sci U S A *118*.

Han, X., Zhou, Z., Fei, L., Sun, H., Wang, R., Chen, Y., Chen, H., Wang, J., Tang, H., Ge, W.*, et al.* (2020). Construction of a human cell landscape at single-cell level. Nature *581*, 303-309.

Hu, M., Yang, B., Cheng, Y., Radda, J.S.D., Chen, Y., Liu, M., and Wang, S. (2020). ProbeDealer is a convenient tool for designing probes for highly multiplexed fluorescence in situ hybridization. Sci Rep *10*, 22031.

Huang da, W., Sherman, B.T., and Lempicki, R.A. (2009). Systematic and integrative analysis of large gene lists using DAVID bioinformatics resources. Nature protocols *4*, 44-57.

Hubstenberger, A., Courel, M., Benard, M., Souquere, S., Ernoult-Lange, M., Chouaib, R., Yi, Z., Morlot, J.B., Munier, A., Fradet, M.*, et al.* (2017). P-Body Purification Reveals the Condensation of Repressed mRNA Regulons. Mol Cell *68*, 144-157 e145.

Huttelmaier, S., Zenklusen, D., Lederer, M., Dictenberg, J., Lorenz, M., Meng, X., Bassell, G.J., Condeelis, J., and Singer, R.H. (2005). Spatial regulation of beta-actin translation by Src-dependent phosphorylation of ZBP1. Nature *438*, 512-515.

Jan, C.H., Williams, C.C., and Weissman, J.S. (2014). Principles of ER cotranslational translocation revealed by proximity-specific ribosome profiling. Science *346*, 1257521.

Kedersha, N.L., Gupta, M., Li, W., Miller, I., and Anderson, P. (1999). RNA-binding proteins TIA-1 and TIAR link the phosphorylation of eIF-2 alpha to the assembly of mammalian stress granules. The Journal of cell biology *147*, 1431-1442.

Keene, J.D. (2007). RNA regulons: coordination of post-transcriptional events. Nature reviews Genetics *8*, 533-543.

Khong, A., Matheny, T., Jain, S., Mitchell, S.F., Wheeler, J.R., and Parker, R. (2017). The Stress Granule Transcriptome Reveals Principles of mRNA Accumulation in Stress Granules. Mol Cell *68*, 808-820 e805.

Kim, D., Paggi, J.M., Park, C., Bennett, C., and Salzberg, S.L. (2019). Graph-based genome alignment and genotyping with HISAT2 and HISAT-genotype. Nat Biotechnol *37*, 907-915.

Küspert, M., Murakawa, Y., Schäffler, K., Vanselow, J.T., Wolf, E., Juranek, S., Schlosser, A., Landthaler, M., and Fischer, U. (2015). LARP4B is an AU-rich sequence associated factor that promotes mRNA accumulation and translation. Rna *21*, 1294-1305.

Lawrence, J.B., and Singer, R.H. (1986). Intracellular localization of messenger RNAs for cytoskeletal proteins. Cell *45*, 407-415.

Lecuyer, E., Yoshida, H., Parthasarathy, N., Alm, C., Babak, T., Cerovina, T., Hughes, T.R., Tomancak, P., and Krause, H.M. (2007). Global analysis of mRNA localization reveals a prominent role in organizing cellular architecture and function. Cell *131*, 174-187.

Lee, S.H., and Mayr, C. (2019). Gain of Additional BIRC3 Protein Functions through 3'-UTR-Mediated Protein Complex Formation. Mol Cell *74*, 701-712 e709.

Lerner, R.S., Seiser, R.M., Zheng, T., Lager, P.J., Reedy, M.C., Keene, J.D., and Nicchitta, C.V. (2003). Partitioning and translation of mRNAs encoding soluble proteins on membrane-bound ribosomes. Rna *9*, 1123-1137.

Liao, Y., Smyth, G.K., and Shi, W. (2014). featureCounts: an efficient general purpose program for assigning sequence reads to genomic features. Bioinformatics *30*, 923-930.

Litterman, A.J., Kageyama, R., Le Tonqueze, O., Zhao, W., Gagnon, J.D., Goodarzi, H., Erle, D.J., and Ansel, K.M. (2019). A massively parallel 3' UTR reporter assay reveals

relationships between nucleotide content, sequence conservation, and mRNA destabilization. Genome Res *29*, 896-906.

Liu, X., and Fagotto, F. (2011). A method to separate nuclear, cytosolic, and membrane-associated signaling molecules in cultured cells. Science signaling *4*, pl2.

Lykke-Andersen, J., and Wagner, E. (2005). Recruitment and activation of mRNA decay enzymes by two ARE-mediated decay activation domains in the proteins TTP and BRF-1. Genes Dev *19*, 351-361.

Ma, W., and Mayr, C. (2018). A Membraneless Organelle Associated with the Endoplasmic Reticulum Enables 3'UTR-Mediated Protein-Protein Interactions. Cell *175*, 1492-1506 e1419.

Ma, W., Zheng, G., Xie, W., and Mayr, C. (2021). In vivo reconstitution finds multivalent RNA-RNA interactions as drivers of mesh-like condensates. eLife *10*.

Martin, M. (2011). Cutadapt removes adapter sequences from high-throughput sequencing reads. 2011 *17*, 3.

Mazan-Mamczarz, K., Lal, A., Martindale, J.L., Kawai, T., and Gorospe, M. (2006). Translational repression by RNA-binding protein TIAR. Mol Cell Biol *26*, 2716-2727.

Meyer, C., Garzia, A., Mazzola, M., Gerstberger, S., Molina, H., and Tuschl, T. (2018). The TIA1 RNA-Binding Protein Family Regulates EIF2AK2-Mediated Stress Response and Cell Cycle Progression. Mol Cell *69*, 622-635 e626.

Mili, S., Moissoglu, K., and Macara, I.G. (2008). Genome-wide screen reveals APC-associated RNAs enriched in cell protrusions. Nature *453*, 115-119.

Miller, S., Yasuda, M., Coats, J.K., Jones, Y., Martone, M.E., and Mayford, M. (2002). Disruption of dendritic translation of CaMKIIalpha impairs stabilization of synaptic plasticity and memory consolidation. Neuron *36*, 507-519.

Moor, A.E., Golan, M., Massasa, E.E., Lemze, D., Weizman, T., Shenhav, R., Baydatch, S., Mizrahi, O., Winkler, R., Golani, O*., et al.* (2017). Global mRNA polarization regulates translation efficiency in the intestinal epithelium. Science *357*, 1299-1303.

Moretti, F., Rolando, C., Winker, M., Ivanek, R., Rodriguez, J., Von Kriegsheim, A., Taylor, V., Bustin, M., and Pertz, O. (2015). Growth Cone Localization of the mRNA Encoding the Chromatin Regulator HMGN5 Modulates Neurite Outgrowth. Mol Cell Biol *35*, 2035-2050.

Navarrete-Perea, J., Yu, Q., Gygi, S.P., and Paulo, J.A. (2018). Streamlined Tandem Mass Tag (SL-TMT) Protocol: An Efficient Strategy for Quantitative (Phospho)proteome Profiling Using Tandem Mass Tag-Synchronous Precursor Selection-MS3. Journal of proteome research *17*, 2226-2236.

Patel, R.K., West, J.D., Jiang, Y., Fogarty, E.A., and Grimson, A. (2020). Robust partitioning of microRNA targets from downstream regulatory changes. Nucleic Acids Res *48*, 9724-9746.

Peeples, W., and Rosen, M.K. (2021). Mechanistic dissection of increased enzymatic rate in a phase-separated compartment. Nature chemical biology *17*, 693-702.

Qin, W., Myers, S.A., Carey, D.K., Carr, S.A., and Ting, A.Y. (2021). Spatiotemporally-resolved mapping of RNA binding proteins via functional proximity labeling reveals a mitochondrial mRNA anchor promoting stress recovery. Nature communications *12*, 4980.

Rappsilber, J., Mann, M., and Ishihama, Y. (2007). Protocol for micro-purification, enrichment, pre-fractionation and storage of peptides for proteomics using StageTips. Nature protocols *2*, 1896-1906.

Reid, D.W., and Nicchitta, C.V. (2012). Primary role for endoplasmic reticulum-bound ribosomes in cellular translation identified by ribosome profiling. J Biol Chem *287*, 5518-5527.

Shin, Y., and Brangwynne, C.P. (2017). Liquid phase condensation in cell physiology and disease. Science *357*.

Smalec, B.M., Ietswaart, R., Choquet, K., McShane, E., West, E.R., and Churchman, L.S. (2022). Genome-wide quantification of RNA flow across subcellular compartments reveals determinants of the mammalian transcript life cycle. bioRxiv, 2022.2008.2021.504696.

Staudacher, J.J., Naarmann-de Vries, I.S., Ujvari, S.J., Klinger, B., Kasim, M., Benko, E., Ostareck-Lederer, A., Ostareck, D.H., Bondke Persson, A., Lorenzen, S.*, et al.* (2015). Hypoxia-induced gene expression results from selective mRNA partitioning to the endoplasmic reticulum. Nucleic Acids Res *43*, 3219-3236.

Stoecklin, G., Colombi, M., Raineri, I., Leuenberger, S., Mallaun, M., Schmidlin, M., Gross, B., Lu, M., Kitamura, T., and Moroni, C. (2002). Functional cloning of BRF1, a regulator of ARE-dependent mRNA turnover. EMBO J *21*, 4709-4718.

Tushev, G., Glock, C., Heumuller, M., Biever, A., Jovanovic, M., and Schuman, E.M. (2018). Alternative 3' UTRs Modify the Localization, Regulatory Potential, Stability, and Plasticity of mRNAs in Neuronal Compartments. Neuron *98*, 495-511 e496.

Vaquerizas, J.M., Kummerfeld, S.K., Teichmann, S.A., and Luscombe, N.M. (2009). A census of human transcription factors: function, expression and evolution. Nature reviews Genetics *10*, 252-263.

Voigt, F., Zhang, H., Cui, X.A., Triebold, D., Liu, A.X., Eglinger, J., Lee, E.S., Chao, J.A., and Palazzo, A.F. (2017). Single-Molecule Quantification of Translation-Dependent Association of mRNAs with the Endoplasmic Reticulum. Cell reports *21*, 3740-3753.

Wang, Z., Kayikci, M., Briese, M., Zarnack, K., Luscombe, N.M., Rot, G., Zupan, B., Curk, T., and Ule, J. (2010). iCLIP predicts the dual splicing effects of TIA-RNA interactions. PLoS Biol *8*, e1000530.

Xia, C., Fan, J., Emanuel, G., Hao, J., and Zhuang, X. (2019). Spatial transcriptome profiling by MERFISH reveals subcellular RNA compartmentalization and cell cycle-dependent gene expression. Proc Natl Acad Sci U S A *116*, 19490-19499.

Yan, X., Hoek, T.A., Vale, R.D., and Tanenbaum, M.E. (2016). Dynamics of Translation of Single mRNA Molecules In Vivo. Cell *165*, 976-989.

Zarnegar, B.J., Flynn, R.A., Shen, Y., Do, B.T., Chang, H.Y., and Khavari, P.A. (2016). irCLIP platform for efficient characterization of protein-RNA interactions. Nat Methods *13*, 489-492.

Zhao, W., Zhang, S., Zhu, Y., Xi, X., Bao, P., Ma, Z., Kapral, Thomas H., Chen, S., Zagrovic, B., Yang, Yucheng T.*, et al.* (2021). POSTAR3: an updated platform for exploring post-transcriptional regulation coordinated by RNA-binding proteins. Nucleic Acids Research *50*, D287-D294.